博士論文番号：9981034

Crystal structures of rat GTP cyclohydrolase I complexed with its feedback regulatory protein, GFRP

（ラットGTPシクロヒドロレースIとそのフィードバック調節蛋白質GFRPとの複合体の結晶構造）

真板　宣夫

奈良先端科学技術大学院大学
バイオサイエンス研究科　生体高分子構造学講座
（箱嶋　敏雄　教授）

２００２年３月提出

Ph. D. thesis

Crystal structures of rat GTP cyclohydrolase I complexed with its feedback regulatory protein, GFRP

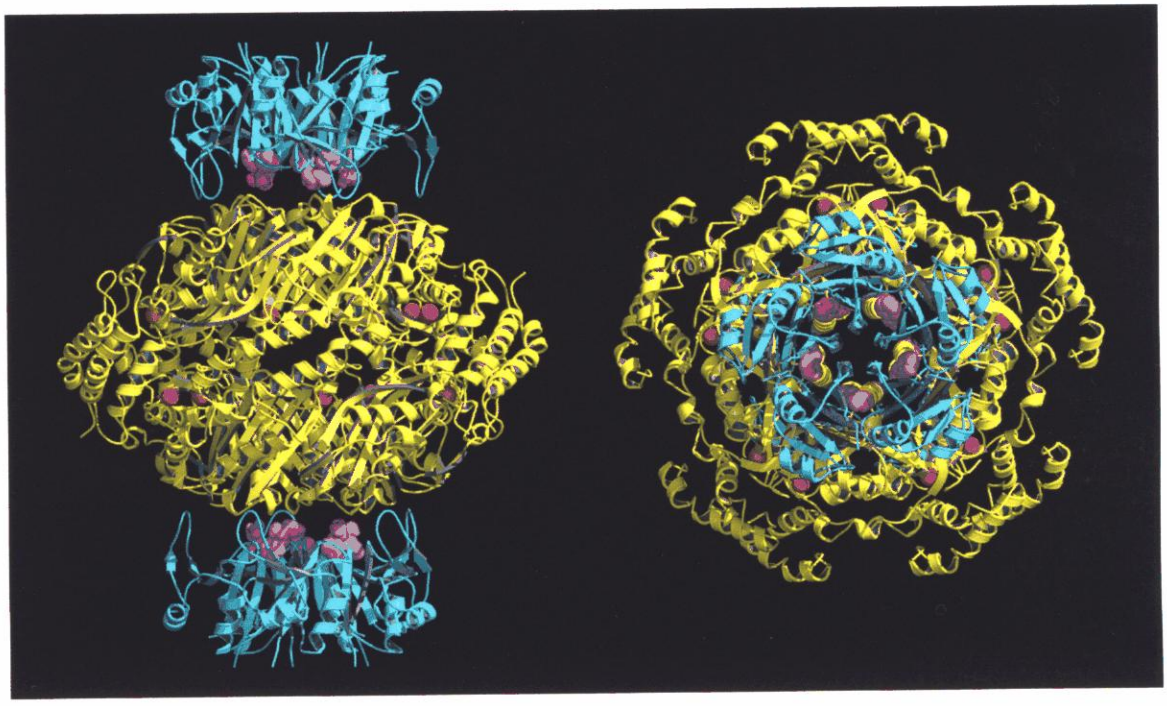

Nobuo Maita

Department of Molecular Biology

Nara Institute of Science and Technology

(Prof. Toshio Hakoshima)

February 2002

Table of Contents

RESULTS

Structural Basis of the GTPCHI-GFRP Complex

Comparison of the Stimulatory and Inhibitory Complexes

DISCUSSION

Discussion

Introduction

1-1. Historical Overview of GTP cyclohydrolase I

GTP cyclohydrolase I (GTPCHI, EC 3.5.4.16) catalyses the formation of D-*erythro*-7,8-dihydroneopterin triphosphate (NH_2P3) and formic acid from GTP. This is the first step in the *de novo* biosynthesis of tetrahydrobiopterin (BH_4) (Fig. 1-1). First, existence of this enzyme was indicated by the observation of release of formic acid from GTP [Burg & Brown, 1966; Burg & Brown, 1968].

To date, *GTPCHI* genes are reported in many species, i.e. *Escherichia coli*, *Dictyostelium discoideum*, *Caenorhabditis elegans*, *Homo sapiens*, *Rattus norvegicus*, *Saccharomyces cerevisiae* and *Drosophila melanogaster* [ExPASy server, Swiss Institute of Bioinformatics]. The comparison of amino acid sequences reveals that the C-terminal half is evolutionary conserved (Fig. 1-3), while the N-terminal half is not. Especially, the N-terminal half of mammalian GTPCHI is different from those from bacteria.

1-2. Reaction Scheme Catalysed by GTPCHI

Apart from most GTP-substrate enzymes, GTPCHI does not

hydrolyse the γ-phosphate nor require a magnesium ion. As shown in figure 1-2, this complicated reaction goes through two steps; ring opening and formic acid release, and Amadori rearrangement followed by the ring closure [Wolf & Brown, 1969](Fig. 1-2). From the early years, it is suggested that in the reaction scheme of the guanine ring opening, the C8 atom of GTP is released as formic acid, followed by Amadori rearrangement [Burg & Brown, 1968].

Ring opening and formic acid release (Fig. 1-2, step 1-5): The guanine ring-opening step is believed to be initiated by nucleophilic attack of a polarized water molecule to the C8 atom of guanine. Then another polarized water molecule again attacked on the C8 atom and formic acid is released. Until the discovery of an essential zinc ion at the catalytic centre, this step had been considered as a critical step, because of a high potential barrier in the ring opening reaction [Nar *et al.*, 1995b; Auerbach *et al.*, 2000]. Recent studies revealed that the zinc ion is necessary for the enzyme activity, and that this ring-opening step is not rate-determining [Auerbach *et al.*, 2000; Schramek *et al.*, 2001]. The finding of a zinc ion at catalytic centre has helped to understand the ring-opening mechanisms. That is because the zinc ion serves as a powerful to the C8 atom of guanine catalyst by

providing an activated water molecule for the nucleophilic attack [McCall *et al.*, 2000].

Amadori rearrangement and ring closure (Fig. 1-2, step 7-11): After formic acid has released, the intermediate compound which prone to have the Amadori rearrangement. From crystallographic studies, it is suggested that histidine provides a proton to the franose O4' atom, resulting in ring opening and generating a Schiff's base [Nar *et al.*, 1995b; Bracher *et al.*, 1998]. Then the rearrangement of the carbohydrate side chain is occurred, followed by the formation of the pyrazine ring of the product. The *Amadori* rearrangement and the following steps are suggested occur spontaneously, as enzyme-independent because of its slow reaction rate [Thöny *et al.*, 2000; Bracher *et al.*, 2001]. These reactions are known to occur without catalysis under physiological conditions.

1-3. GTPCHI Feedback Regulatory Protein

A phenomenon of inhibition of the rat GTPCHI activity by reduced pterins was first reported in 1984 [Bellahsene *et al.*, 1984; Shen *et al.*, 1988]. In case of bacterial GTPCHI, however, no inhibition had been observed [Yim & Brown, 1976; Jackson & Shiota,

1975]. At that time, and the presence of another protein was not recognized. In 1993, Harada *et al.* first reported GTPCHI forms a complex with a co-factor protein and to exhibit feedback-regulation behaviour [Harada *et al.*, 1993]. They also showed that the formation of the complex requires effector molecules, L-phenylalanine for the stimulatory complex formation, and BH_4 and GTP for the inhibitory complex formation. In 1996, Milstein *et al.* reported the DNA sequence of the rat co-factor protein, and this novel 10kDa protein was termed as **G**TPCHI **F**eedback **R**egulatory **P**rotein, GFRP [Milstein *et al.*, 1996]. Milstein and co-workers predicted that the GFRP exist as a dimmer by judging from gel filtration [Milstein *et al.*, 1996], but Yoneyama *et al.* had done a cross-linking study and concluded that it was not a dimer but a pentamer [Yoneyama *et al.*, 1997].

To date, several features of this peculiar protein are found. I) The GFRP gene is found only mammals such as in human, rat and mouse but no homological genes are found in bacteria, plants, yeast and *Drosophila*. In bacteria and plants, NH_2P3 serves as an intermediate in the biosynthesis of tetrahydrofolate [Brown & Williamson, 1987]. II) In the stimulatory or inhibitory complexes, phenylalanine weakly binds to GFRP but not to GTPCHI, and on the

contrary, BH_4 weakly binds to GTPCHI but not to GFRP [Yoneyama & Hatakeyama 2001].

1-4. Structural Study of GTPCHI

The structural studies of bacterial GTPCHI have been carried out by Huber and co-workers. It had been shown by biochemical experiments that GTPCHI forms a high molecular mass complex while the number of components was undefined, because of high molecular mass. The first reliable result was brought about by freeze-etching electron microscopy [Meining *et al.*, 1995] and x-ray diffraction: Nar *et al.* had presented the crystal structure of *E. coli* GTPCHI at 3.0 Å [Nar *et al.*, 1995a] (Fig. 1-4,1-5). *E. coli* GTPCHI folds into and α+β structure with the helical N-terminal segments, which contains an antiparalell helix pair remote from the rest of the molecule. This pair gears with the opposite GTPCHI ring. The C-terminal segment of the monomer is formed by a central four-stranded antiparallel β-sheets. The β-sheets gathered from five monomers forms a β-barrel core in the pentameric ring (Fig. 1-4).

Interestingly, this structural fold is common in purin- or pterin-substrate enzyme, such as 6-pyruvoyl tetrahydropterin

synthase, urate oxidase and dihydroneopterin aldolase. All these enzymes form a homo-oligomeric ring and double doughnuts structure, and the active sites are located at the interface of two subunits. These architectures of this family are termed as T-fold [Nar *et al.*, 1995a; Colloc'h *et al.*, 2000].

To date, following GTPCHI structures are registered to the Protein Data Bank: *E. coli* GTPCHI (1GTP) [Nar *et al.*, 1995a], *E. coli* GTPCHI (H112S Mutant) +GTP (1A8R), *E. coli* GTPCHI (C110S Mutant) +GTP (1A9C), *E. coli* GTPCHI +Zn (1FBX) and human GTPCHI +Zn (1FB1) [Auerbach *et al.*, 2000].

1-5. GTPCHI in Diseases

Human GTPCHI has been well characterized as the gene responsible for hyperphenylalaninemia and dopa-responsive dystonia (DRD). In 1994, Ichinose *et al.* mapped the gene for DRD to 14q22.1-q22.2, and identified it as *GTPCH* gene [Ichinose *et al.*, 1994]. DRD is caused by deficiency of dopamine to less than 20% of the normal level in the nigro-striatum of the brain owing to the disorder of dopamine synthesis [Nagatsu & Ichinose, 1998]. After this discovery, many mutations have been reported in DRD patients [Brique *et al.*, 1999].

As described above, GTPCHI is involved in *de novo* biopterin synthesis in human, and biopterin is an important co-factor for neurotransmitter syntheses, including phenylalanine hydroxylase, tyrosine hydroxylase, tryptophan hydroxylase and inducible nitric oxide synthase [Kaufman, 1997; for reviews]. Thus, the decrease of GTPCHI activity are linked to the decrease of BH_4, resulting in the disorder of neurotransmitter such as dopamine, serotonine and nitric oxide (Fig. 1-1).

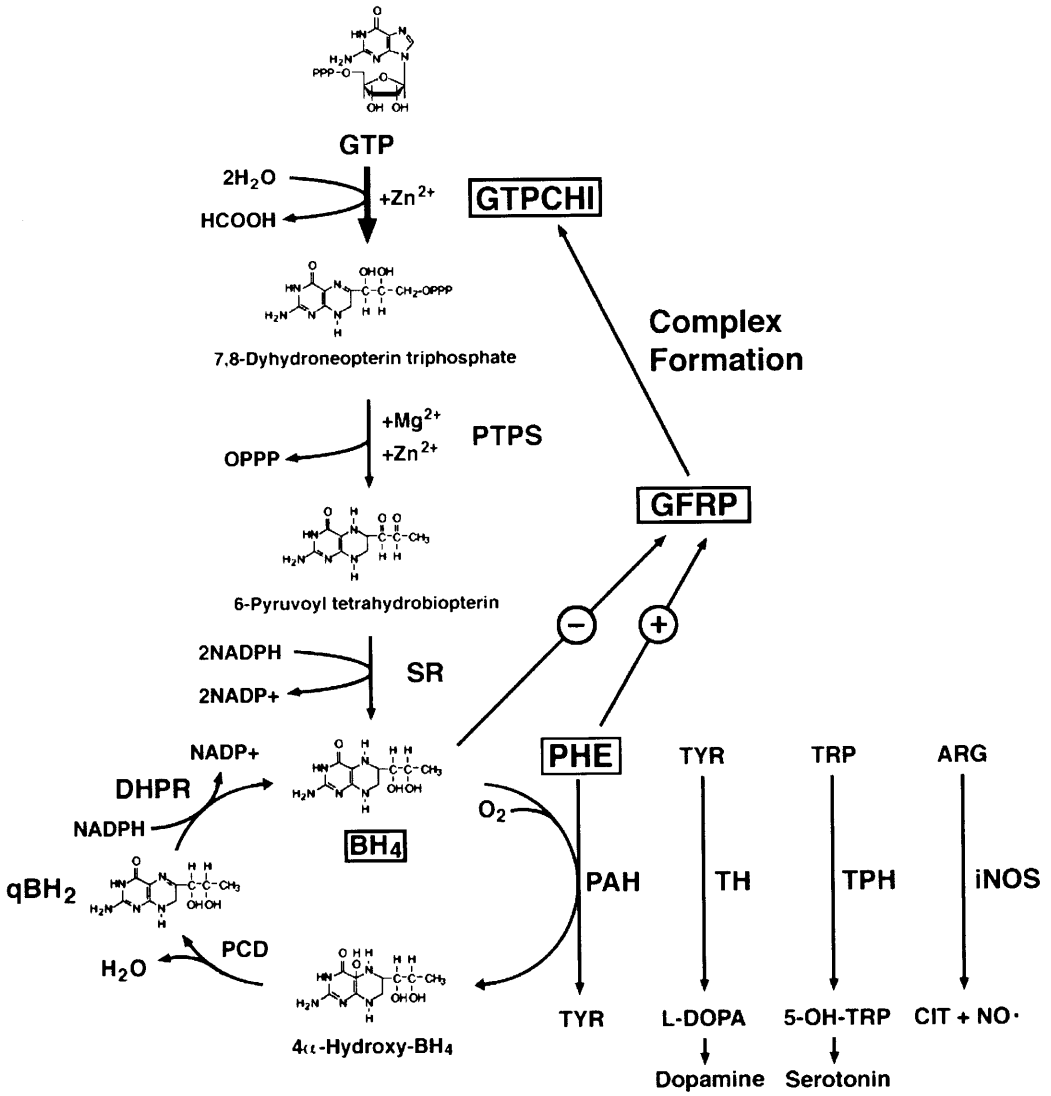

Figure 1-1. The biosynthesis of BH_4 and amino acid hydroxylases reaction requiring BH_4.
Abbreviations are PTPS, 6-pyruvoyl-tetrahydropterin synthase; SR, sepiapterin reductase; PCD, pterin- 4α-carbinolamine dehydratase; DHPR, dihydropteridine reductase; PHE, phenylalanine; TYR, tyrosine; TRP, tryptophan; ARG, arginine; DOPA, 3,4-dihydroxyphenylalanine; CIT, citrulline; PAH, phenylalanine hydroxylase; TH, tyrosine hydroxylase; TPH, tryptophan hydroxylase; iNOS, inducible nitric oxide synthase; qBH_2, quinonoid-dihydrobiopterin.

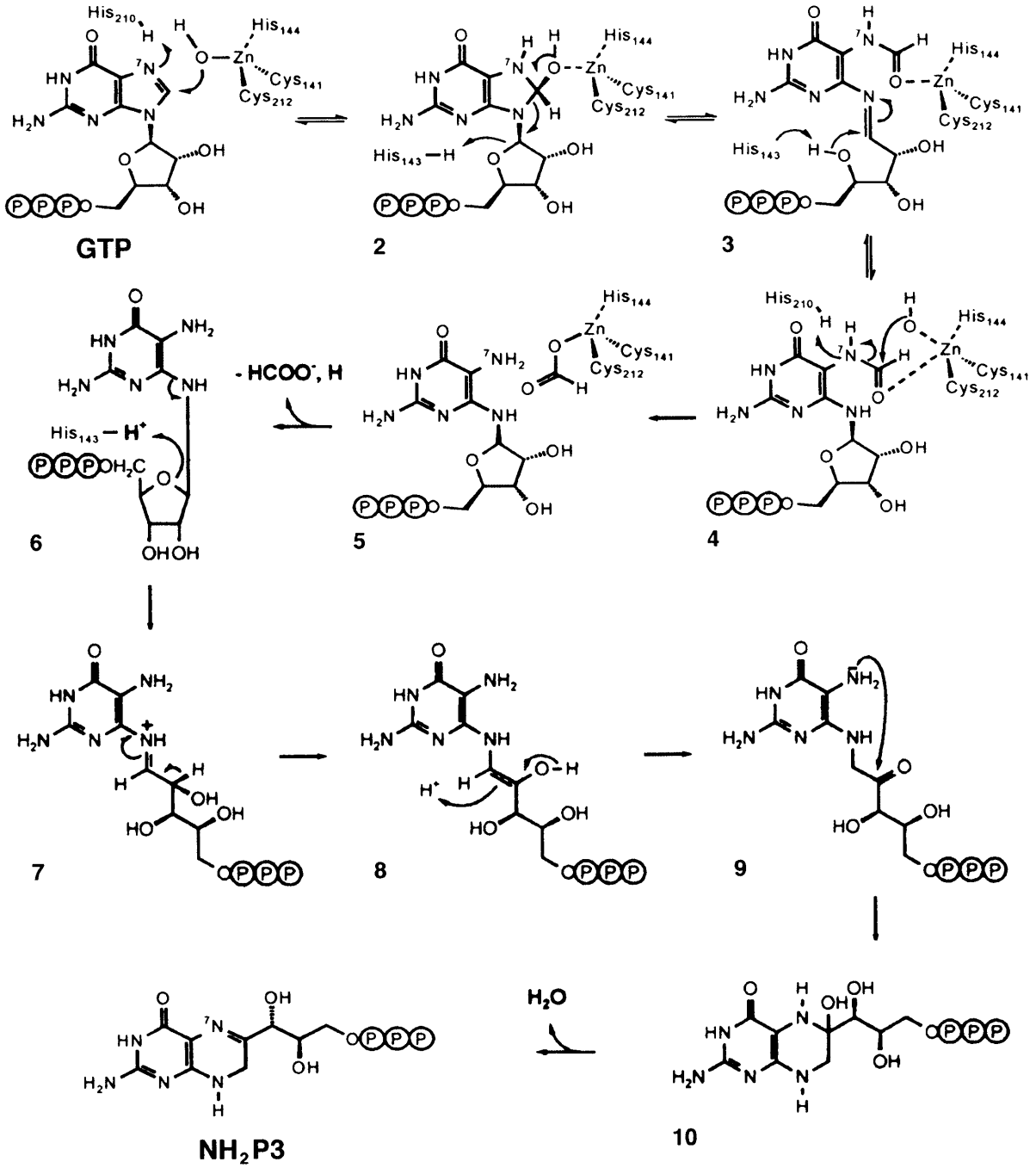

Figure 1-2. Possible reaction scheme catalysed by GTPCHI proposed by Bacher and co-workers [Auerbach *et al.*, 2000; Schramek *et al.*, 2001].

Figure 1-3. Multiple amino-acid sequence alignment of GTPCHI [Thöny *et al.*, 2000]. Identical or homologous residues (V/L/I, R/K, M/L, D/E) are highlighted with magenta. The alignment was generated using CLUSTAL W program [Thompson *et al.*, 1994].

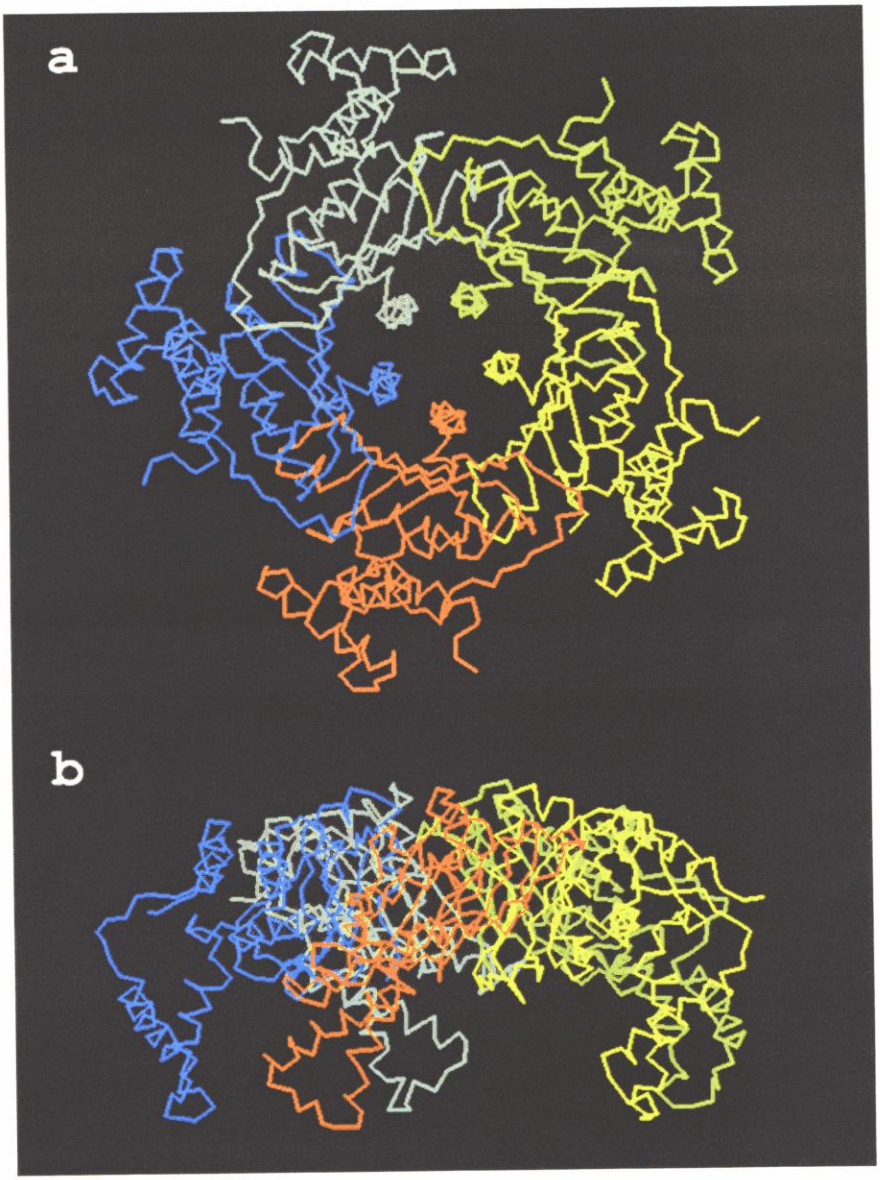

Figure 1-4. Top (a) and side (b) view of C^{α} backbone representation of the *E. coli* GTPCHI (PDB code 1GTP) pentamer [Nar *et al.*, 1995a]. The GTPCHI decamer is formed by two pentameric rings docked face-to-face.

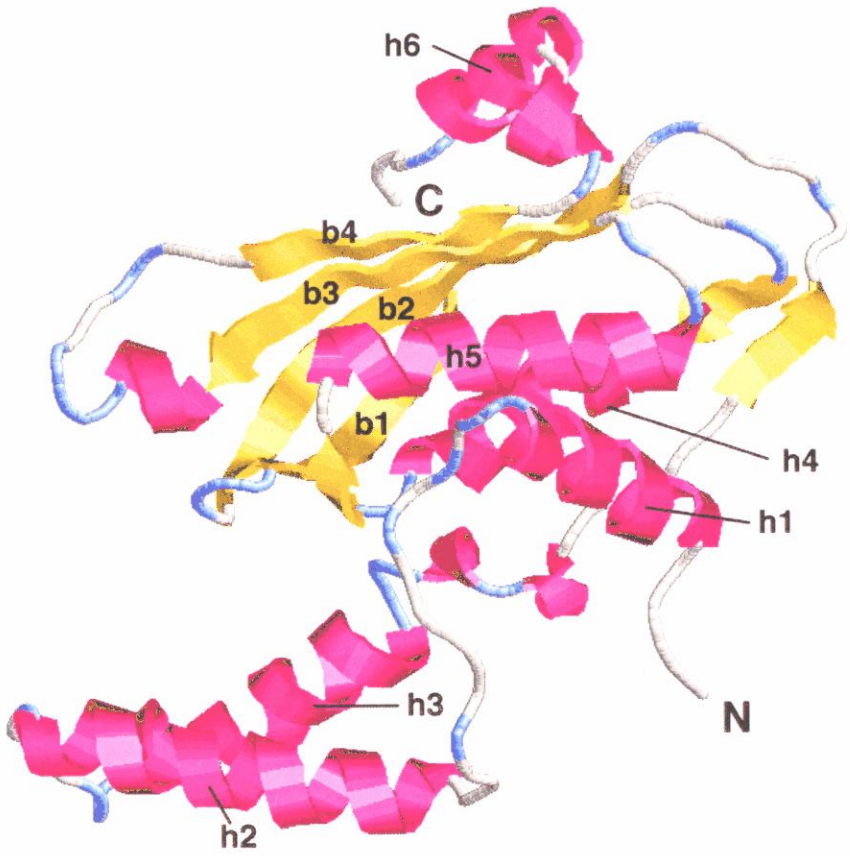

Figure 1-5. Ribbon representation of *E. coli* GTPCHI monomer structure [Nar *et al.*, 1995b].

X-ray Crystallographic Study of the Stimulatory GTPCHI-GFRP Complex

2-1. Sample Preparation

Expression in *E. coli* and purification of recombinant rat GTPCHI and GFRP were carried out by the methods as described [Yoneyama *et al.*, 1997]. Purified GTPCHI was concentrated to 6 mg mL^{-1} in 50 mM Tris-HCl (pH 7.5) containing 0.1 M KCl, 1 mM EDTA and 1 mM DTT. Purified GFRP was concentrated to 5 mg mL^{-1} in 50 mM MES-NaOH (pH 6.0). Both proteins were stored at 193 K for the crystallization study.

The preparation of the stimulatory complex was done as follows. The protein mixture (3.2 mL) containing 50 mM Tris-HCl pH 7.5, 0.1 M KCl, 1 mM phenylalanine, 1 mM EDTA, 15 μM (54 μg mL^{-1}) GTPCHI and 15 μM (20 μg mL^{-1}) GFRP was incubated at 20°C for 20 min and concentrated to a 12 mg mL^{-1} solution by filtration with 100 kDa cutoff Microcon (Millipore, USA). Protein concentration was measured with absorbance spectra with the molar extinction coefficient $\varepsilon_{M,280}$ (= 291,200 M^{-1} cm^{-1}) and the calculated molecular weight (357,363) of complex (see supplemental data). The extinction coefficient (E_{280})

of complex is 1.23 mL mg^{-1} cm^{-1}. One microlitter of condensed protein solution were diluted with 49 μL of 50 mM Tris-HCl (pH 7.5), then measured an absorbance spectra with a Beckman DU 640 spectro-photometer.

2-2. Crystallization of the Stimulatory Complex

Screening of the crystallization conditions of the complex were performed with hanging-drop vapour-diffusion methods [McPherson, 1990], the droplets were made as 1 μL of protein solution (5 mg mL^{-1}) mixed with 1 μL of reservoir solution. The CrystalScreen I, II, GridScreen Kits (Hampton Research, USA) were used for the first screening of crystallization conditions. Tiny, wedge-shaped crystals were observed in a droplet containing 64 % MPD, 0.1 M Tris-HCl (pH 8.0). Several attempts to grow better crystals with micro- and/or macro-seeding techniques made possible to obtain the large crystals with the volume of over 0.2 x 0.2 x 0.2 mm^3. The crystals were analysed by SDS polyacrylamide gel electrophoresis (SDS-PAGE) [Laemmli, 1970] and confirmed to contain the GTPCHI-GFRP complex (Fig. 2-2).

The optimised crystallization condition was obtained as follows. The initial drop was made by mixing 1 μL of a protein

solution (12 mg mL^{-1}) with 1 μL of a MPD solution [47.5% (v/v) MPD, 5 mM phenylalanine, and 0.1 M Tris-HCl (pH 7.5)] including several microseeds. The drop was vapour-diffused against 0.5 mL of reservoir solution [35 % (v/v) MPD, 5 mM phenylalanine, and 0.1 M Tris-HCl (pH 7.5)] at 283 K. The complex crystals usually appeared within 12 hours and grew to its maximum size in a week (Fig. 2-1a). For the microscopic seeding, the proper size (~0.1 mm) of crystals were picked up and transferred to a 40 % (v/v) MPD solution (~200 μL) and then crashed with a homogeniser, followed by centrifugation to remove the supernatant (~100 μL). All operations were done at 4°C. To control the nucleus number, serially diluted 40 fold with 47.5 % (v/v) MPD solutions.

The crystals were also appeared when using PEG 300 and IPA instead of MPD (Fig. 2-1b,c,d). However, crystals grown in PEG300 solution poorly diffracted and the crystals obtained from IPA (or ethanol) were fragile.

2-3. Data Collection

To prevent the radiation damage during data collection, crystals were flash-frozen at 100 K [Hope, 1988] with 30 % (v/v) MPD solutions as a cryo-protectant. The first dataset (3.0 Å) were

collected at the beam-line BL-6A of the Photon Factory (Table 2-2). The diffraction data were processed with the *DENZO/SCALEPACK* package [Otwinowski, 1996]. The crystals were found to belong to monoclinic space group $P2_1$ with unit-cell dimensions a = 123.3, b = 111.4, c = 125.8 Å, β = 97.69°. Assuming the presence of one complex in the asymmetric unit, the calculated value of the crystal volume per protein mass (V_M) [Matthews, 1968] is 2.39 $Å^3$ Da^{-1}. This value corresponds to a solvent content of approximately 49 %.

Self-rotation functions were calculated with *POLARFRN* [Rossmann & Blow, 1962] to look for non-crystallographic symmetry (NCS) with several Patterson sphere radii. These analyses revealed a strong peak (51.6 % height of the origin peak) in κ = 72°, representing a non-crystallographic five-fold axis (Fig. 2-3 left) and also peaks representing five two-fold axes perpendicular to the five-fold axis (Fig. 2-3 right). A close inspection of the section κ = 180° of the self-rotation function revealed a diffuse peaks between each pair of strong peaks. These peaks may suggest that five two-fold axes of GFRP are shifted from those of GTPCHI by a rotation around the five-fold axis. These results indicate that the asymmetric unit contains decamers of GTPCHI and GFRP with pseudo D_5 symmetry.

Using the *E. coli* GTPCHI structure [PDB code 1GTP, Nar *et al.*, 1995a], rotation functions were calculated with *AMoRE* [Navaza, 1994], giving me the ten distinct solutions that clearly represented D_5 symmetry (Table 2-1). However, the calculated electron density map was too poor to trace the C^{α} backbone of GFRP, even using density modification techniques.

2-4. Preparation and Data Collection of Heavy-Atom Derivatives

To obtain more precise experimental phases, Se-Met-substituted GFRP was prepared. In addition, heavy-atom derivatives were screened by soaking method. Since the crystals were stable in 40 % (v/v) MPD solution, several solutions containing 1 mM heavy-atom in 40 % (v/v) MPD, 5 mM phenylalanine and 0.1 M Tris-HCl (pH 7.5) were prepared. The soaking studies were done using VDX plates with 500 μL of 40 % MPD solution (depleted of heavy-atom) as a reservoir solution. A droplet of 5 μL heavy-atom solution was put on a siliconized glass plate, followed by transferring the crystals to the droplet then sealed with grease. The VDX plate was placed in the cold room (4°C) for 3 to 13 hours. The soaked crystals were rapid frozen with liquid nitrogen for X-ray diffraction experiments with a Rigaku-FR roting anode X-ray generator. The resolution limit

of the data were 3.2 Å, but was enough for determination of the initial phases.

Results of the heavy-atom derivative search are summarized in Table 2-3. The data reduction and integration were done with the program *DENZO/SCALEPACK* [Otwinowski & Minor, 1997], and then the output data file was translated to the CCP4 format (MTZ file), followed by processing with the programs *SORTMTZ*, *TRUNCATE* and *CAD* [CCP4, 1994]. The derivative data were merged with native data, and scaled together with the program *SCALEIT* [CCP4, 1994]. The difference Patterson map was calculated with the program *FFT* [CCP4, 1994], and then visualized with the program *NPO* [CCP4, 1994]. The data of the crystal, soaked for 13 hours with methylmercurychloride (CH_3MgCl) gave the specific peaks derived from heavy-atoms in Harker section (Fig. 2-4a).

As the spacegroup $P2_1$ has only one Harker section, the mercury sites could not determined unequivocally. The positions of the mercury atoms were calculated with the MR phases from the alanine-substituted model of decameric *E. coli* GTPCHI, and the difference Fourier map was generated. The highest thirty peaks were marked with the program *PEAKMAX* [CCP4, 1994], then displayed with the computer graphic program *O* [Jones et al., 1991], viewed along

five-fold axis of *E. coli* GTPCHI. As the heavy-atoms were expected to bind to specific sites of each subunit, the heavy-atoms were likely arranged with five-fold symmetry. Ten mercury atoms were found in the asymmetric unit and 5 out of 10 mercury atoms were related by the 5-fold rotation axis with ~15 Å apart (Fig. 2-4b). Several mercury-atoms were on the surface of the unit cell, so that the cross-peaks appeared in Harker-section were overlapped (Fig. 2-4a).

Se-Met derivative crystals were prepared by the same procedure as that for native crystals using Se-Met GFRP instead of native GFRP. The x-ray diffraction data of Se-Met derivatives were collected at the beam-line BL41XU in the SPring-8, with maximum resolution of 2.8 Å (Table 2-2). Since the GFRP has five methionine residues per subunit, 50 selenium sites should be found in asymmetric unit. In generals, Se-Met derivative is used for the multiple wavelength anomalous dispersion (MAD) method [Hendrickson, 1991]. Since experimental phases had been already obtained from the MR method and the Hg derivative, Se-Met were used as a heavy-atom for conventional MIR methods. The Se-Met data collected at BL41XU of SPring-8 were processed with the programs *MOSFLM* [Leslie, 1999] and *SCALA* [CCP4, 1994]. Using the phases calculated from 10 mercury

atoms, 27 out of 50 selenium sites were found in the asymmetric unit.

2-5. Phase Determination, Model Building and Structure Refinement

Heavy-atom positions, occupancies, *B*-factors and initial phases were calculated and refined with the program *MLPHARE* [CCP4, 1994]. Although the initial experimental phases calculated from 10 mercury and 27 selenium atoms were good enough for tracing the region of GFRP, the density modification, including non-crystallographic symmetry (NCS) averaging, histogram matching and solvent flattening, and phase extension greatly improved the phases and produced an excellent electron density map. At this stage, most of the GFRP residues could be built unambiguously with *O*. The detailed phasing statistics were summarized in table 2-2.

The structure refinement was carried out with the program *CNS* [Brünger *et al.*, 1998] using the selenomethionyl derivative data at 2.8 Å. Rounds of manual rebuilding and structure refinement using maximum-likelihood target gave a final refined model of the stimulatory complex with an *R* factor of 22.8 % (free-*R* factor of 26.4 %), including 2,780 amino acids of the GTPCHI-GFRP complex, 10 phenylalanines, 142 water molecules, and 10 tentative potassium

ions, but a 2Fo-Fc map containing poor peaks for possible zinc ions at the active sites.

To establish the presence of zinc ions at the active sites, dataset was collected from the complex crystals that were prepared with a GTPCHI sample purified without EDTA. The presence of zinc ions was confirmed by fluorescence XAFS measurements (Fig. 2-5). The positions of zinc ions were identified by a difference Fourier map using a λ_{peak} (λ=1.282 Å) data. Structural refinements against this data to an *R*-factor of 21.6 % (R_{free} 24.3 %) revealed 10 zinc ions at every 10 active sites. All residues of GFRP were ordered in the electron density map, whereas the 36 N-terminal residues (residues 12-47) and two residues (Val^{209} and Gln^{210}) of GTPCHI were not visible on the current map, probably due to disorder. In the refined structure of the selenomethionyl derivative, Gln^{80} of GTPCHI was replaced with Ala. Structural refinement against the heavy-atom data of CH_3HgCl revealed that the mercury atoms were bound to Cys^{80} of GFRP.

Ramachandran plot analyses (Fig. 2-8a,b) revealed that two GTPCHI residues (Leu^{108} and Lys^{151}) and one GFRP residue (Ile^{10}) are in disallowed region.

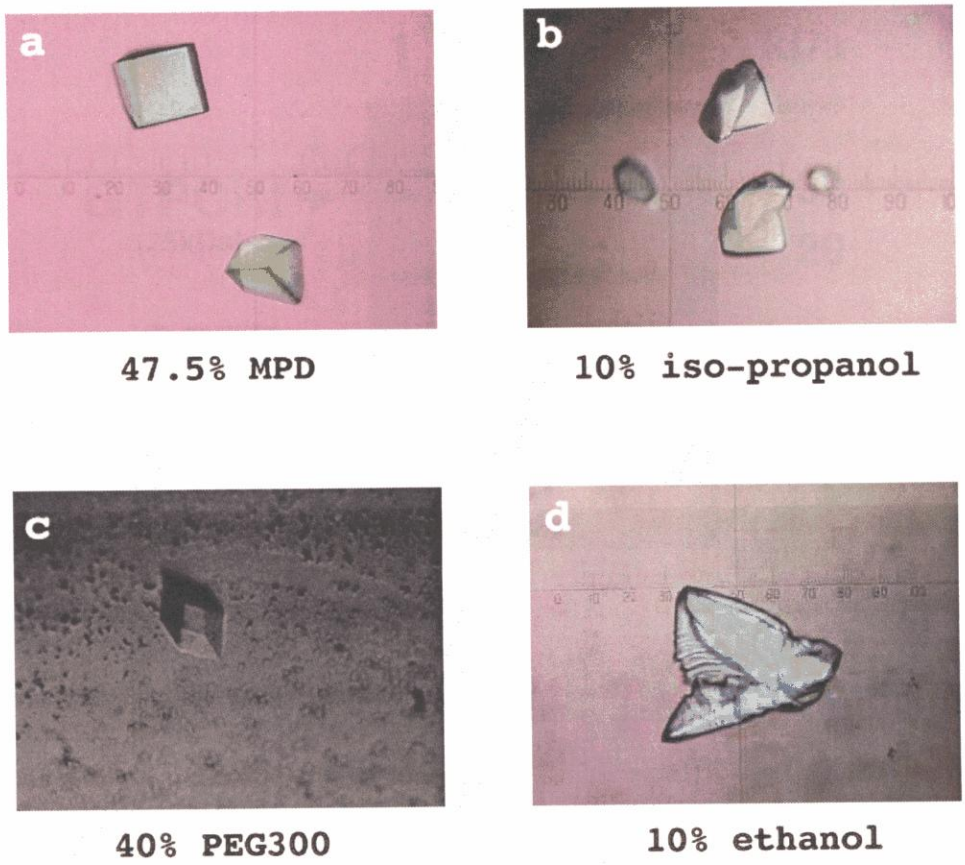

Figure 2-1. The crystals of the stimulatory GTPCHI-GFRP complex. All crystals were grown in 0.1 M Tris-HCl (pH 7.5). GTPCHI-GFRP crystals were prone to grown when using the organic solvent as participitant, such as MPD (a), IPA (b), PEG300 (c) or ethanol (d). Only MPD crystals were durable enough for the diffraction data collection.

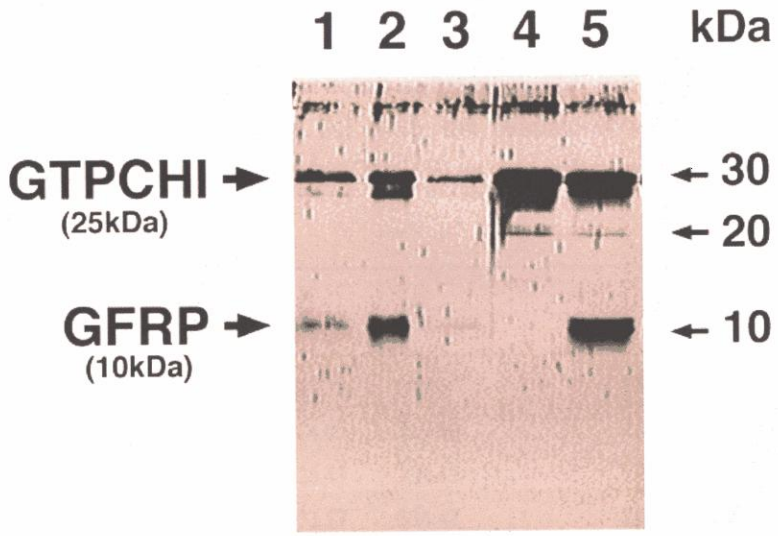

Figure 2-2. Silver-stained SDS-PAGE (16.5 % gel) analysis of the stimulatory GTPCHI-GFRP complex. lane 1:twice-washed crystals, lane 2:the crystallization droplet solution, lane 3: crystal-washed buffer, lane 4: GTPCHI control (1 μg), lane 5:GTPCHI (1 μg) and GFRP (0.3 μg) control.

Table 2-1. Results of the rotation function analyses calculated with the native data (10-4 Å) with the alanine-substituted *E. coli* GTPCHI structure (residue 28-219) as a search model.

	α	β	γ	Corr-F
1	252.01	105.31	39.60	25.2
2	287.99	74.69	219.60	25.2
3	141.61	126.43	154.42	24.7
4	38.39	53.57	334.42	24.7
5	172.80	132.20	355.50	24.6
6	7.20	47.80	175.50	24.6
7	99.46	98.14	317.44	24.2
8	80.54	81.86	137.44	24.2
9	230.69	120.91	211.13	23.5
10	309.31	59.09	31.13	23.5
11	260.94	98.93	221.88	14.0

Table 2-2. Data Collection and Model Refinement Statistics

	Native	Se-Met	CH_3HgCl	Zinc λ_{peak}
Data collection ¶				
X-ray source	PhotonFactory	SPring-8	Rigaku FR-C	SPring-8
Wavelength (Å)	0.980	1.000	1.542	1.282
Resolution (Å)	3.0 (3.11-3.00)	2.8 (2.94-2.80)	3.5 (3.62-3.50)	2.7 (2.84-2.70)
Reflections (obs)	368, 952	589,690	36,708	693,751
Reflections (uni)	60,761	83,068	2,949	93,244
R_{sym} (%)§	6.8 (25.9)	11.2 (57.8)	13.2 (26.7)	9.5 (28.6)
Completeness (%)	89.4 (72.8)	99.4 (99.4)	85.8 (69.6)	99.9 (99.9)
Phasing				
Resolution range (Å)		15.0-3.1	15.0-3.5	
Heavy atom sites		27	10	
R_{deriv} (%) ‡		16.9	4.2	
R_{Cullis} (cent/acent) (%)*		0.92 / 0.94	0.90 / 0.81	
Phasing power (cent/acent) †		0.45 / 0.64	0.88 / 1.19	
Overall figure of merit	0.79			
Model refinement				
Resolution range (Å)		15.0-2.8		15-2.7
R_{work}/R_{free}-values (%) ‖		22.8 / 26.3		21.6 / 24.3
B_{ave} (Å^2)		58.1		42.6
Bond length rmsD (Å)		0.0081		0.0082
Bond angle rmsD (°)		1.35		1.39
Protein atoms		22,120		22,000
Ligands (Phe) atoms		120		120
Solvent and ion atoms		140		392

¶ Statistics for the outer shell are given in parentheses.

§ $R_{sym} = \Sigma| I - < I > | / \Sigma I$, where I is the integrated intensity for a particular reflection.

‡ $R_{deriv} = \Sigma||F_{derivative}| - |F_{native}|| / \Sigma|F_{native}|$.

* $R_{Cullis} = \Sigma||F_{PH}| \pm |F_P| - |F_{H|calc}| / \Sigma||F_{PH}| \pm |F_P||$, where F_{PH}, F_P and F_H are the scaled structure factors of the derivative, native and heavy atom, respectively.

† Phasing power = $< F_H > / <$ lack of closure $>$.

‖ $R_{work/free} = \Sigma||F_O| - |F_C|| / \Sigma|F_O|$, where F_O and F_C are the observed and calculated structure factor amplitudes. 5% of the reflections were excluded from working set for calculating free-*R* value.

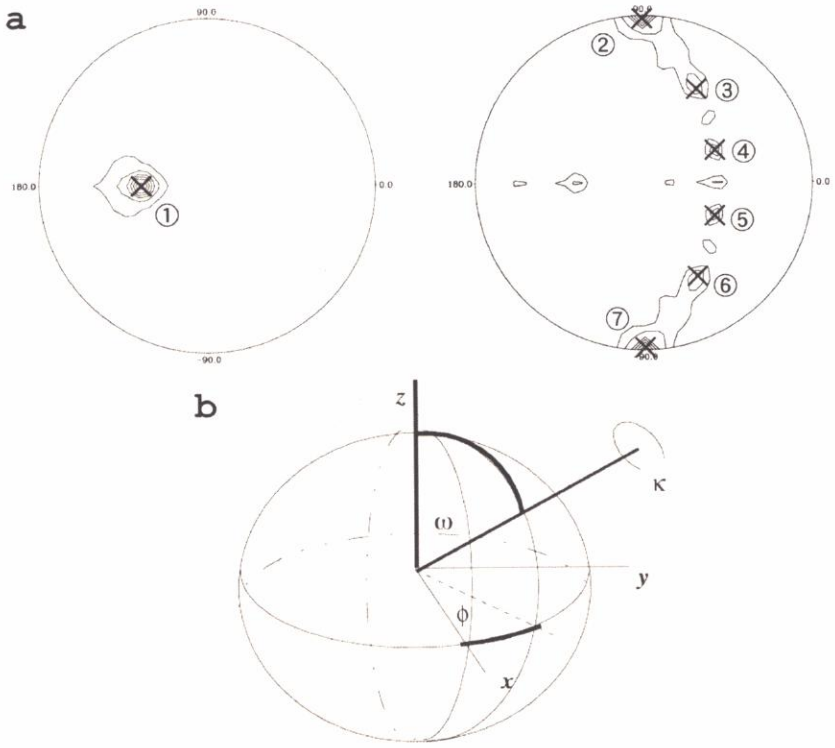

Figure 2-3. (a) Self-rotation functions and the symmetry of the stimulatory complex. Stereographic projection of the section κ = 72° (left) and the section κ = 180° (right) of the self-rotation function of the stimulatory GTPCHI/GRP/Phe complex. The integration radius in the Patterson space is 35 Å and data are included from 15 Å to 5 Å. Contouring starts at the 2σ level and the interval is 1σ. The *c** axis is perpendicular to each projection, in which φ = 0°, 90°, 180° and -90° are indicated with the *a* axis along φ = 0°. In left figure, the peak 1 at ω = 137.5°, φ = 180° corresponds to the non-crystallographic five-fold axis. In right figure, five peaks Five peaks are marked by crosses with peak numbers; 2 (ω = 90.0°, φ = 90.0°), 3 (66.6°, 63.0°), 4 (49.6°, 24.9°), 5 (49.6°, 335.1°), 6 (66.6°, 297.0°) and 7 (90.0°, 270.0°). These peaks are separated by 36° and correspond to the non-crystallographic two-fold axes perpendicular to the five-fold axis. (b) Definition of the polar angle.

Table 2-3. Heavy-Atom Derivative Searching Study Results

Heavy Atom	Soaking Time	X-ray data	R_{deriv} / $_{weighted}$-R (%) (Resolution) (Å)	Results
1mM $Pt(CN_4)_2$	1 hour	low resolution (≥9Å)		
1mM K_2HgI_4	1 hour	OK	20.2 / 1.7 (15 - 4)	no heavy-atom
1mM K_2HgI_4	13 hours	Cell has changed to C2 (161 112 123, β=130°)		
5mM K_2PtCl_4	3.8 hours	Cell has changed to C2 (161 110 122, β=121°)		
1mM $KAuCl_4$	15 hours	OK	30.7 / 0.8 (15 - 4)	no heavy-atom
1mM $K_2Pt(NO_2)_4$	13 hours	low isomorphous (124 112 127, β=98°)	25.7 / 1.0 (15 - 4)	
1mM CH_3HgCl	13 hours	OK	25.7 / 3.3 (15 - 3.5)	*strong peak has observed in Harker section.*

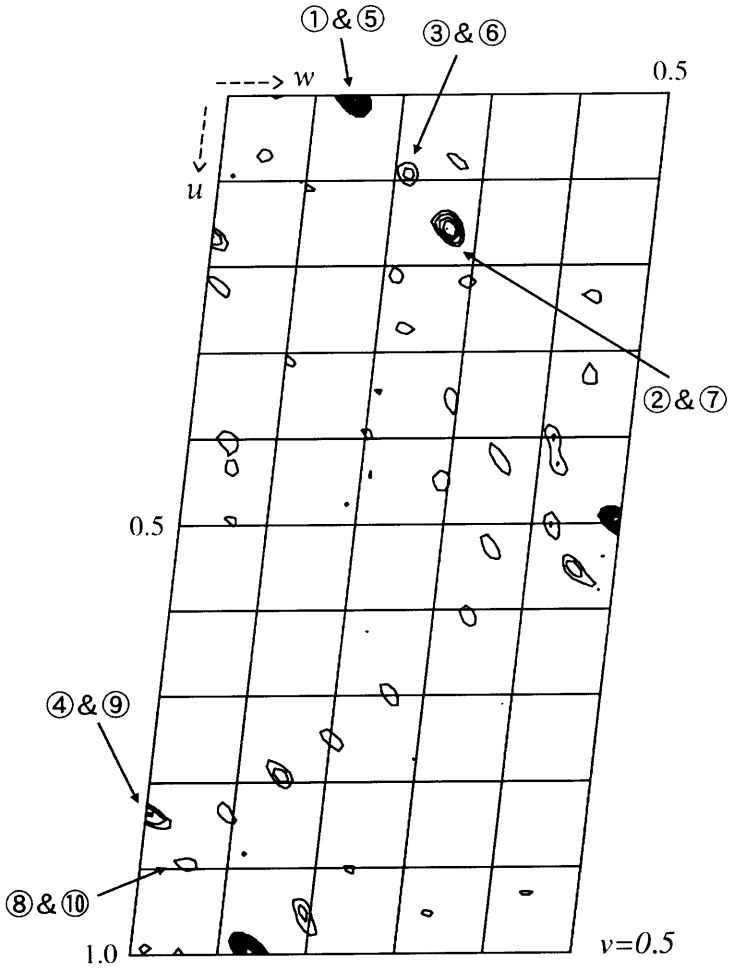

Figure 2-4a. A Harker section (v = 0.5) of a difference Patterson map between CH_3HgCl and Native data. Contouring starts at the 2σ level and the interval is 1σ. The positions of mercury atom were determined by MR (see text), and identified on the map. All peaks derived heavy-atom were overlapped of two mercury atoms. Numbers indicated in are corresponding with figure 2-4b.

cell 122.356 111.547 124.339 90.000 97.309 90.000 P21
Hg position (fractional coordinate)

①	0.500	0.121	-0.076
②	0.082	0.022	0.633
③	0.050	-0.103	0.606
④	0.582	0.047	-0.001
⑤	0.001	0.104	0.577
⑥	0.449	-0.080	-0.108
⑦	0.419	0.045	-0.134
⑧	0.551	-0.078	-0.026
⑨	-0.083	0.033	0.501
⑩	-0.052	-0.095	0.525

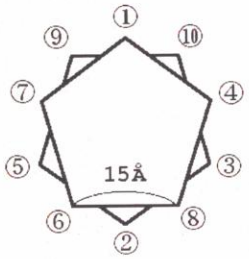

Figure 2-4b. The determined ten mercury sites and their positional relationship. Ten mercury atoms are arranged as two orthogonal pentagons, which has a side of 15 Å long. Each pentagon is about 100 Å apart.

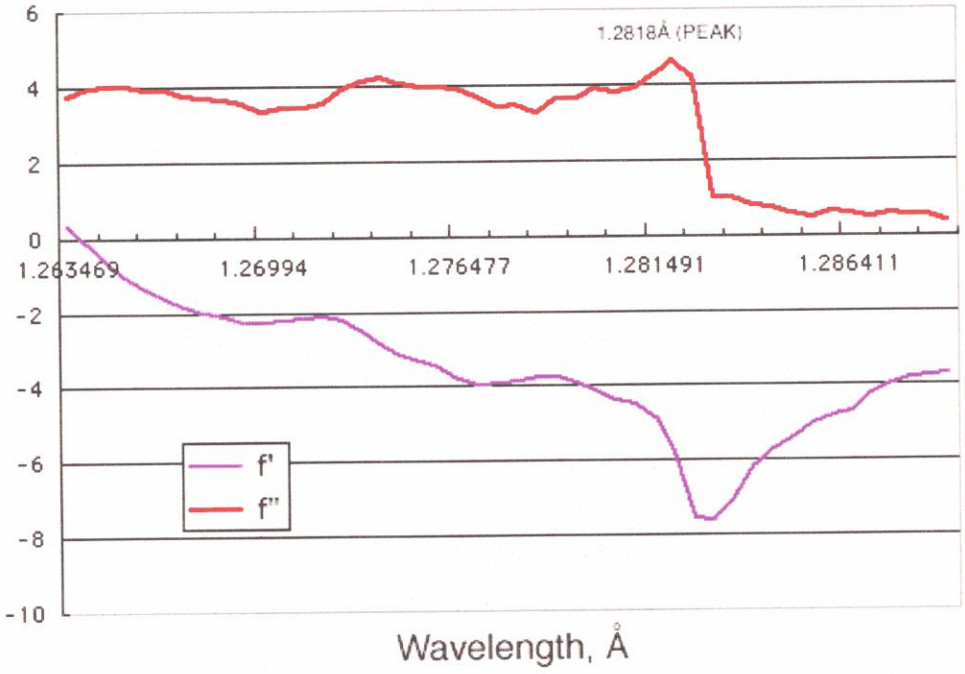

Figure 2-5. Fluorescence XAFS spectrum around K-absorption peak for zinc atom. The crystal obtained from GTPCHI purified with EDTA-free solution and GFRP was mounted on goniometer in BL41XU at SPring-8, and then collected fluorescence with scanning wavelength. An obvious shift of scattering factor (f″) at λ=1.282 Å, which is critical evidence for the presence of zinc atoms in the crystal.

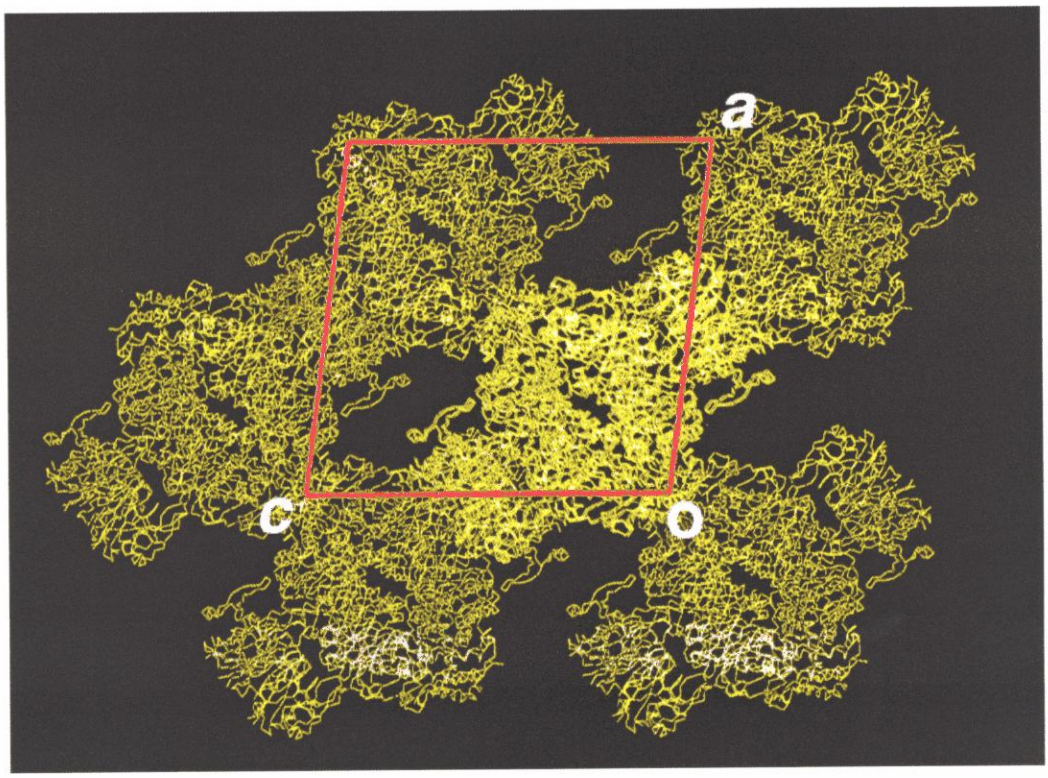

Figure 2-6. Crystal packing of the stimulatory GTPCHI-GFRP complex ($P2_1$), viewed along *b* axis. One complex is in the asymmetric unit. The figure is made by *O* [Jones, *et al.*,1991].

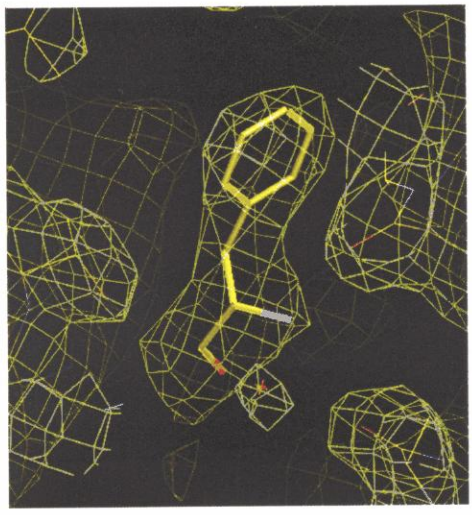

Figure 2-7. 2Fo-Fc electron density around the liganded phenylalanine molecule. The map is contoured at 1.4σ. The figure is made by *O* [Jones, *et al.*, 1991].

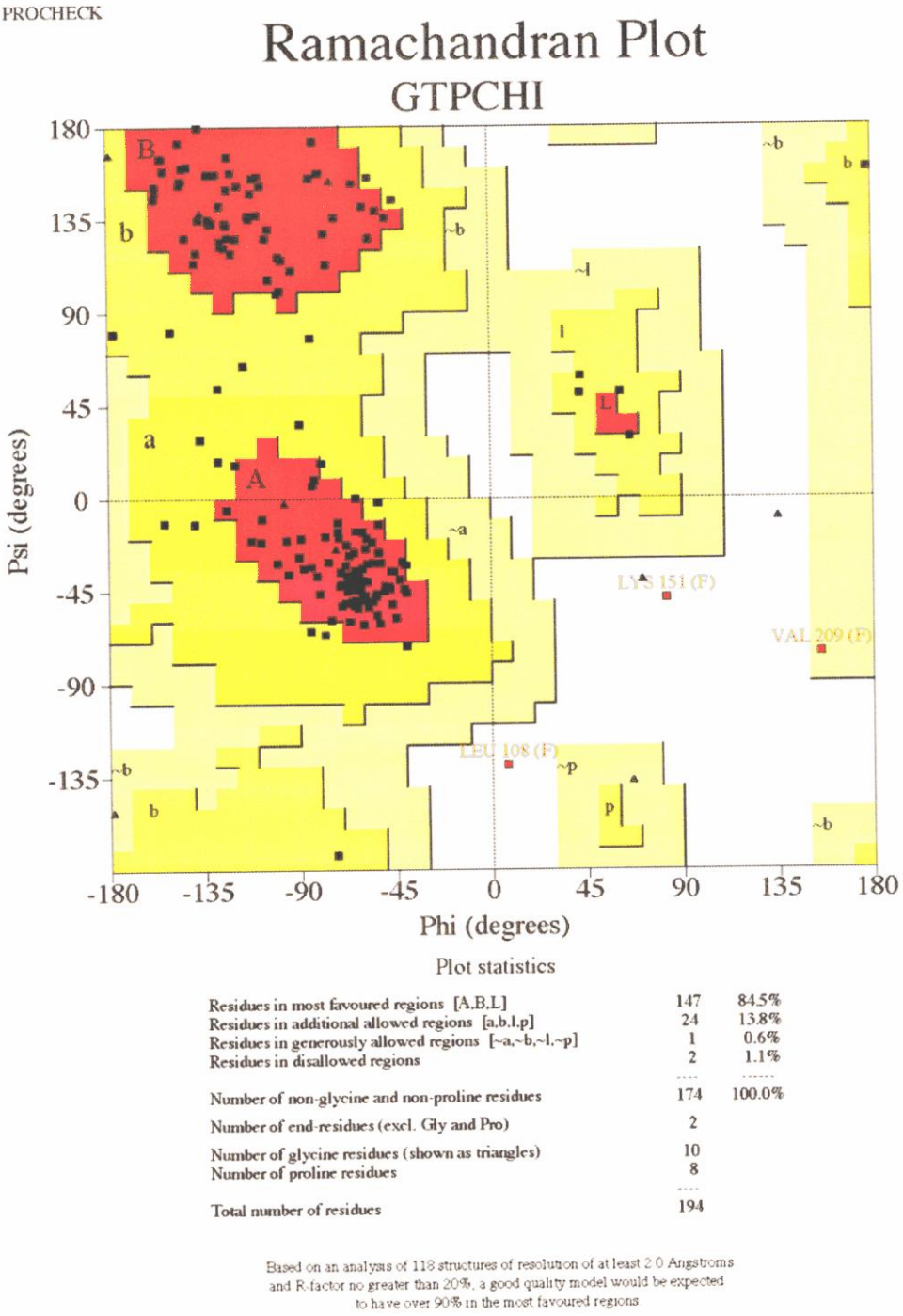

Figure 2-8a. Ramachandran plot of the stimulatory GTPCHI subunit (48-241), calculated with the program *PROCHECK* [Laskowski *et al.*, 1993].

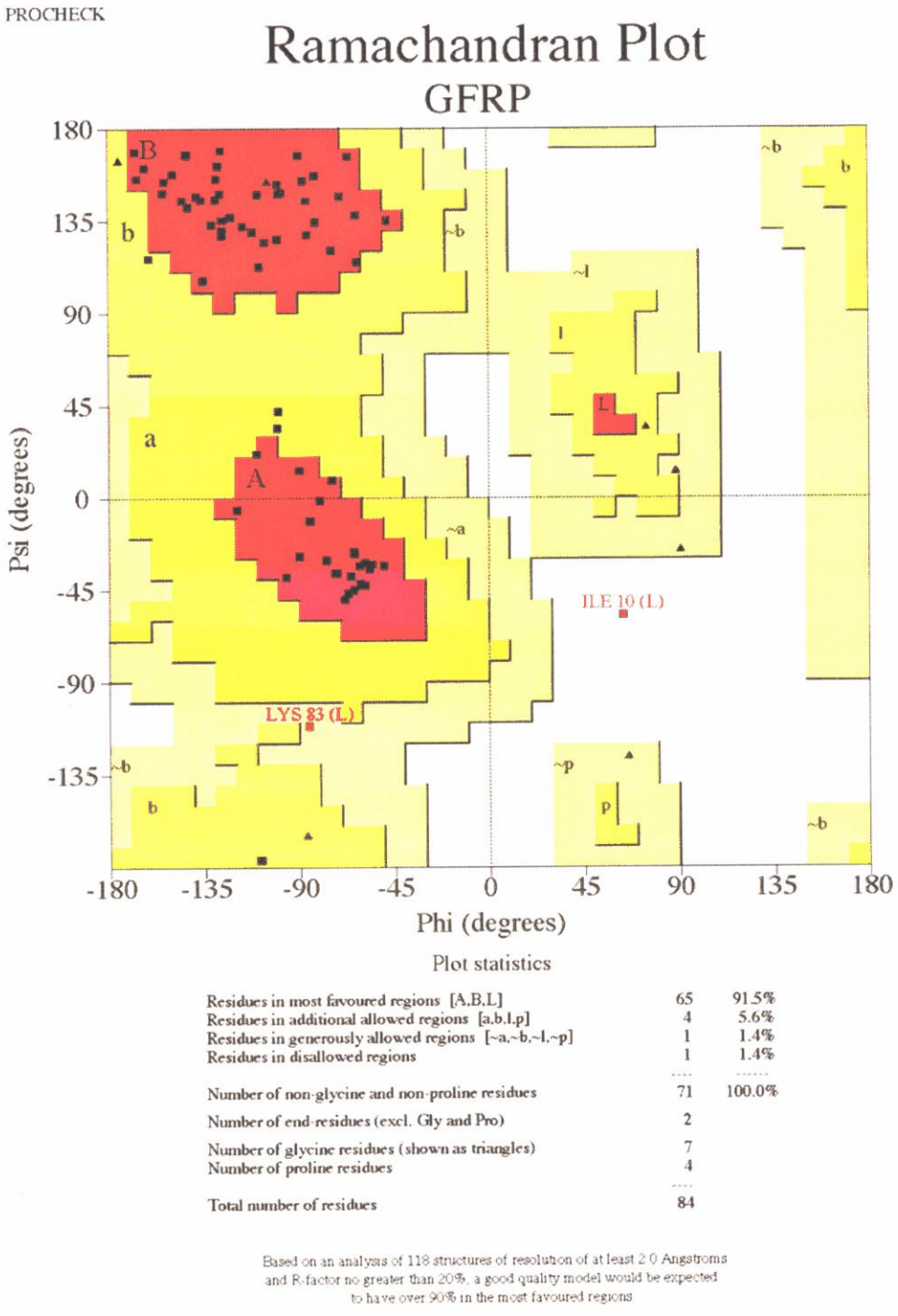

Figure 2-8b. Ramachandran plot of the stimulatory GFRP subunit (1-84), calculated with the program *PROCHECK* [Laskowski *et al.*, 1993].

X-ray Crystallographic Study of the Inhibitory GTPCHI-GFRP Complex

3-1. Sample Preparation

Expression in *E. coli* and purification of recombinant rat GTPCHI and GFRP were carried out by the methods previously described [Yoneyama *et al.*, 1997]. Purified GTPCHI was concentrated up to 6 mg mL^{-1} in 50 mM Tris-HCl buffer (pH 7.5) including 100 mM KCl, 1 mM EDTA, and 1 mM DTT, and purified GFRP was condensed up to 5 mg mL^{-1} in 50 mM MES-NaOH buffer (pH 6.0). Both protein samples were stored at 193 K for the crystallization study. To prepare the inhibitory complex, 6.4 mL of protein mixture [15 μM GTPCHI, 15 μM GFRP, 100 mM NaCl, 1 mM EDTA, 3 mM DTT, 0.3 mM deoxy GTP, 45 μM BH_2, 50 mM MES-NaOH (pH 6.0)] was incubated at room temperature for 20 min, followed by a concentration up to 10 mg mL^{-1} with Microcon-100 (Millipore, USA). BH_4 is easily oxidized and transformed into BH_2, and the efficiency of BH_2 for the complex formation is the same order as that of BH_4 [Shen *et al.*, 1988; Yoneyama & Hatakeyama, 1998]. Therefore, BH_2 was used as analogue molecules of BH_4 for the crystallization. For similar reasons,

deoxy-GTP was used instead of GTP.

3-2. Crystallization of the Inhibitory Complex

The first screening of the crystallization conditions were done with vapour-diffusion technique using CrystalScreen I and II kit (Hampton Research) and several solutions containing ammonium sulfate with methanol, ethanol, *iso*-propanol (IPA), *tert*-butanol, ethylene glycol, dioxane, MPD, 1,6-Hexanediol and PEG300 [Jancarik & Kim, 1991; Huang *et al.*, 1999]. Crystals were obtained from ammonium sulfate solutions containing IPA. The hanging-drop methods gave the round-shaped crystals (Fig. 3-1a), while the sitting-drop methods gave the well, sharpen crystals (Fig. 3-1b). A 8 μL initial droplet [6 mg mL^{-1} protein, and 50 mM MES-NaOH (pH 6.0), 6 % (v/v) IPA, 0.1 M ammonium sulfate and 5 mM β-mercapto-ethanol] was vapour-equilibrated against 0.5 mL of a reservoir solution [100 mM MES-NaOH (pH 6.0), 12 % (v/v) IPA, 0.2 M ammonium sulfate and 10 mM β-mercaptoethanol] at 10°C. Crystals grown under this condition reached their maximum size (0.6 x 0.4 x 0.4 mm^3) within two weeks.

3-3. Data Collection

Crystals were transferred into cryo-protectant solution [14 % IPA, 0.2 M ammonium sulfate, 10 % (v/v) PEG300, 10 % (v/v) ethylene glycol and 0.1 M MES-NaOH (pH 6.0)], and then rapidly frozen by transferring into liquid nitrogen. During the data collection, the atmosphere of crystal was kept at 100 K with a cryo-stream of a liquid N_2 gas. The X-ray diffraction data were collected at the beam-line BL41XU of the SPring-8. After measurements of the X-ray Absorption Fine Structure (XAFS) spectrum, the wavelength for the K-absorption peak of zinc atoms (λ=1.2818 Å) was determined for the peak-data collection (Fig. 2-5). The data collection statistics are shown in table 3-1.

All data were processed with the programs *DPS/MOSFLM* package. The crystals belong to spacegroup $P2_1$ with unit cell dimensions of a = 121.7, b = 109.7, c = 130.3 Å, β = 97.85°. Assuming one GTPCHI decamer and two GFRP pentamers in an asymmetric unit, a Matthews coefficient V_M of 2.33 $Å^3$ Da^{-1} is obtained. This value is within the normal range found for proteins [Matthews, 1968]. The obtained V_M value corresponds to a solvent content of 47.2 %.

In order to find NCS in the complex structure, we calculated self-rotation functions. The κ = 72° and κ = 180° section of the

map calculated with an integration radius of 40 Å using data in a resolution range 10-5 Å are shown in figure 3-2. There is a peak of height 12σ at polar angles ω = 58.1, φ = 180, κ = 72°, corresponding to a five-fold axis (Fig. 3-2 left). In the κ = 180° section of the map, five two-fold axes are observed (Fig. 3-2 right). Each neighbouring pair of these axes had an angle of nearly 36°. In addition, all these two-fold axes were perpendicular to the five-fold axis. This result indicates that the inhibitory complex has pseudo D_5 symmetry as well as the stimulatory complex.

3-4. Model Building and Refinement

The structure was determined by molecular replacement methods using the GTPCHI decamer from the stimulatory complex as a search model. The rotation functions calculated by the program *AMoRe* [Navaza, 1994] with the resolution range of 10-5 Å and an integration vector of 40 Å. Ten solutions showing the same correlation value of 47 % were obtained, which represents D_5 symmetry. The initial coordinates were built with the stimulatory complex. The model was refined with the program *CNS* [Brünger *et al.*, 1998] by several techniques such as rigid-body refinement, stimulated annealing, individual *B*-factor refinement and energy minimization under the NCS restraint on GTPCHI

and GFRP respectively. The final structure consists of one GTPCHI decamer (residues 48-241 for each subunit), two GFRP pentamer (residues 1-84 for each subunit), ten BH_2 molecules, ten zinc ions, ten sodium ions, 291 water molecules and ten triphosphate fragments of the bound deoxy-GTP molecules. The final *R*- and free-*R*-value was 20.7 % and 23.3 %, respectively. The refinement statistics are also shown in table 3-1.

The positions of zinc ions were confirmed using anomalous structure factors with the phases calculated from the refined model. The highest ten peaks corresponding to ten zinc ions at the active sites were arranged as D_5 symmetry.

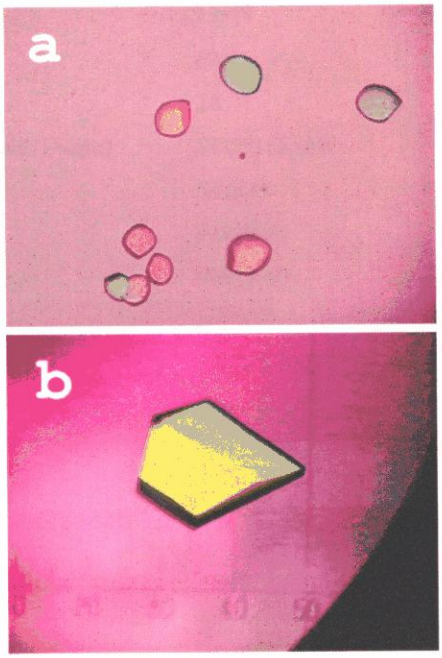

Figure 3-1. Crystals of the inhibitory GTPCHI-GFRP complex obtained by the hanging-drop method (a), and by the sitting-drop methods (b).

Table 3-1. Data Collection and Refinement of the inhibitory GTPCHI-GFRP complex.

Data collection¶		
X-ray source		SPring-8 BL41XU
Wavelength (Å)		1.2818
Spacegroup		$P2_1$
d_{min} (Å)		2.8
Number of Reflections (Observed / Unique)		533,591 / 83,649
Multiplicities		6.4 (6.4)
Completeness (%)		99.9 (99.9)
Anomalous completeness (%)		99.9 (99.9)
Unit cell		a=121.72, b=109.67, c=130.27 Å, β=97.85°
Asymmetric unit cell component		$(GFRP)_5$-$(GTPCHI)_{10}$-$(GFRP)_5$
V_M (Å^3 / Da)		2.46
R_{sym} §(%)		8.9 (38.6)
I/σ (I)		7.6 (1.9)
Refinement		
Resolution range (Å)		15 – 2.8
R / R_{free} †(%)		20.7 / 23.3
No. of non-H Atoms	Protein	22,100
	BH_2/triphosphate	170 / 130
	Water / Zn^{2+} / Na^+	291 / 10 / 10
$B_{average}$ (Å^2)		35.4
R.m.s. deviations	Bond length (Å)	0.0085
	Bond angles (°)	1.417

¶ The values in the parenthesis are statistics of outer shell (2.94-2.80 Å).

§ $R_{sym} = \Sigma_{hkl}\Sigma_i|I_{mean} - I_i| / \Sigma_{hkl}\Sigma_i I_i$

† $R = \Sigma||F_o|-|F_c|| / \Sigma|F_o|$, where F_o and F_c are the observed and calculated structure factor amplitudes. 5% of the reflections were excluded for calculating free-R value.

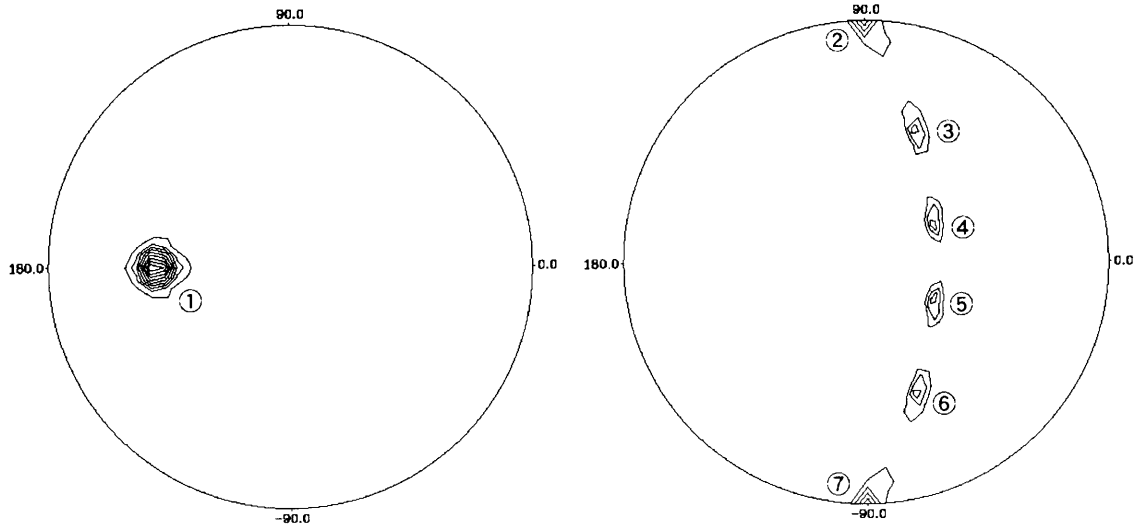

Figure 3-2. Self-rotation function calculated from the diffraction data of the inhibitory GTPCHI-GFRP complex in the resolution range of 10-5 Å with a probe radius of 40 Å. The κ = 72° (*left*) and κ = 180° (*right*) section of the map are indicated. Both maps are contoured at 1σintervals from 3σ. The *c** axis is perpendicular to each projection with the *a* axis along φ = 0°. Each vectors are; 1:(φ, ω, κ) = (58.1, 180, 72), 2:(φ, ω, κ) = (90, 90, 180), 3:(φ, ω, κ) = (59.9, 68.8, 180), 4:(φ, ω, κ) = (35.9, 32.0, 180), 5:(φ, ω, κ) = (35.9, 328.0, 180), 6:(φ, ω, κ) = (59.9, 291.2, 180), 7:(φ, ω, κ) = (90, 270, 180).

Table 3-2a. Results of the rotation function analyses calculated with GTPCHI decamer of stimulatory complex (see text).

	Rotation angle			*R*-factor
	α	β	γ	(%)
1	180.10	57.12	209.74	47.8
2	-0.10	122.88	29.74	47.8
3	179.12	57.62	282.29	46.7
4	0.88	122.38	102.29	46.7
5	180.96	57.79	137.15	46.3
6	-0.96	122.21	317.15	46.3
7	-0.48	121.29	245.50	46.1
8	180.48	58.71	65.50	46.1
9	0.63	121.36	174.19	45.7
10	179.37	58.64	354.19	45.7

Table 3-2b. Results of the translation function analysis.

	Rotation angle			Translation vector			$R_{\text{-factor}}$	Corr-F
	α	β	γ	x	y	z	(%)	
1	180.10	57.12	209.74	0.2500	0.0000	0.2500	39.9	62.7
2	-0.10	122.88	29.74	0.2500	0.0000	0.2500	39.9	62.7
3	179.12	57.62	282.29	0.2500	0.0000	0.2500	39.6	63.0
4	0.88	122.38	102.29	0.2500	0.0000	0.2500	39.6	63.0
5	180.96	57.79	137.15	0.2500	0.0000	0.2500	40.2	62.1
6	-0.96	122.21	317.15	0.2500	0.0000	0.2500	40.2	62.1
7	**-0.48**	**121.29**	**245.50**	**0.2500**	**0.0000**	**0.2500**	**39.6**	**63.8**
8	180.48	58.71	65.50	0.2500	0.0000	0.2500	39.6	63.8
9	0.63	121.36	174.19	0.2500	0.0000	0.2500	39.7	62.3
10	179.37	58.64	354.19	0.2500	0.0000	0.2500	39.7	62.3

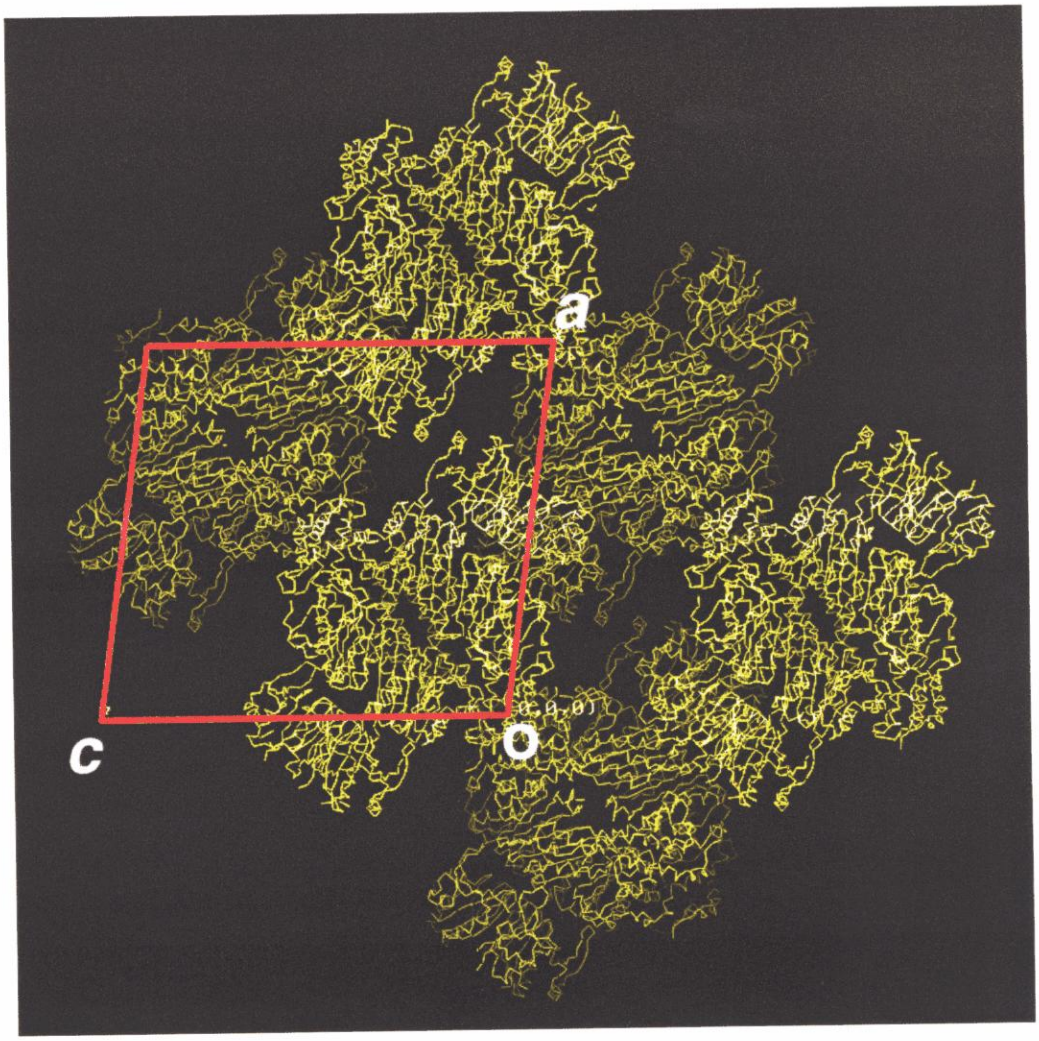

Figure 3-3. Crystal packing of the inhibitory GTPCHI-GFRP complex ($P2_1$), viewed along *b* axis. The figure is made by *O* [Jones, *et al.*, 1991].

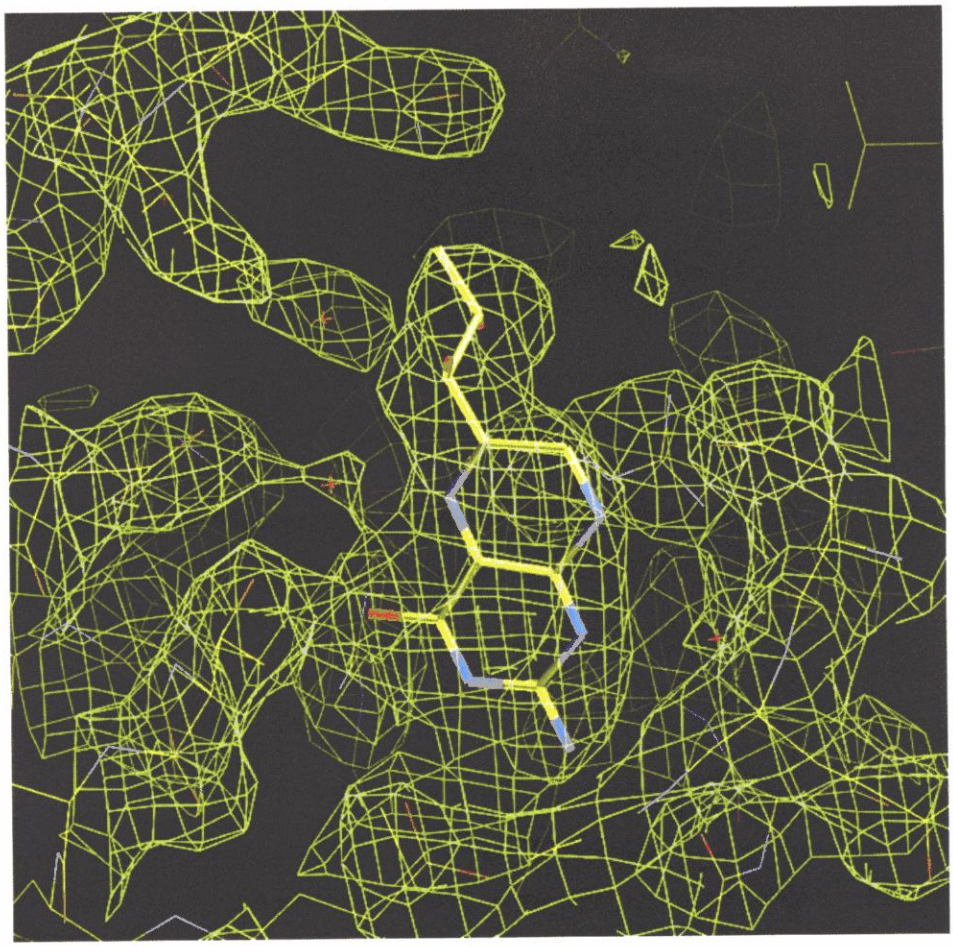

Figure 3-4. Electron density around the liganded BH_2 molecule. The map is contoured at 1.0σ. The figure is made by *O* [Jones, *et al.*, 1991].

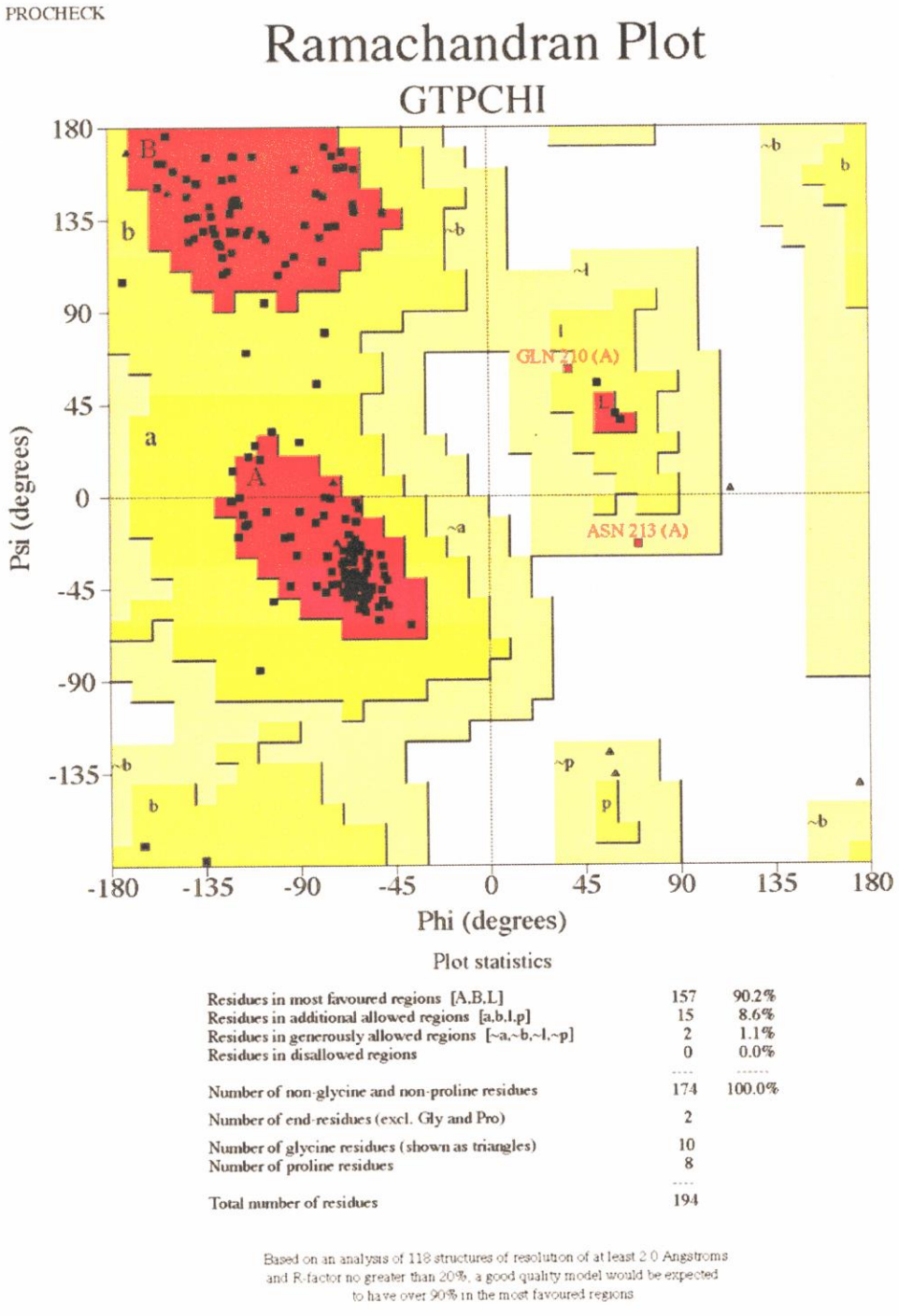

Figure 3-5a. Ramachandran plot of the inhibitory GTPCHI subunit (48-241), calculated with the program *PROCHECK* [Laskowski *et al.*, 1993].

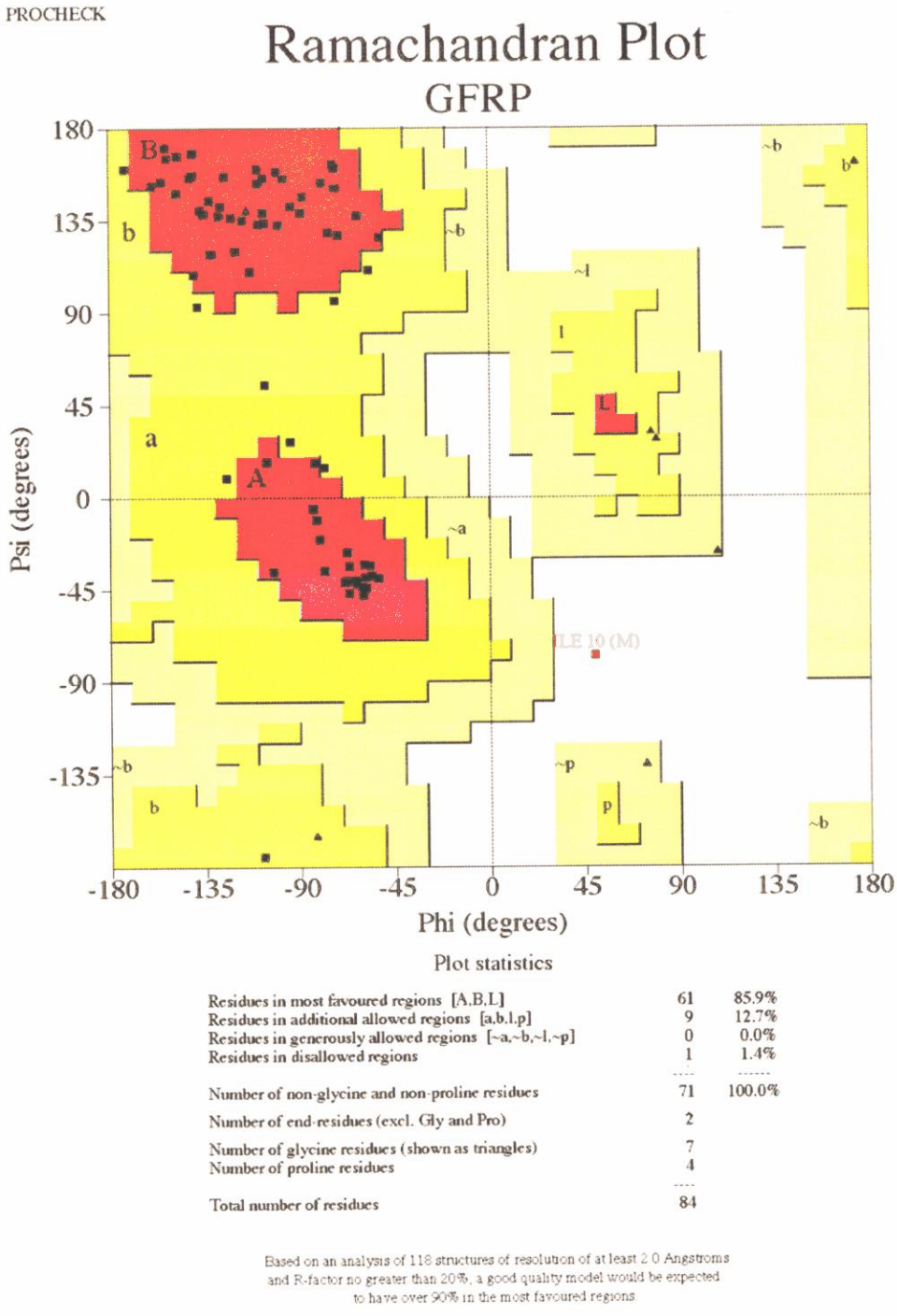

Figure 3-5b. Ramachandran plot of the inhibitory GFRP subunit (1-84), calculated with the program *PROCHECK* [Laskowski *et al.*, 1993].

Structural Basis of the GTPCHI-GFRP Complex

4-1. Overall Structure

The stimulatory complex contains ten phenylalanine molecules in an asymmetric unit. The model includes ten GTPCHI subunits (residues 48-241), ten GFRP subunits (residues 1-84), ten phenylalanine molecules, and ten zinc ions. The 36 residues (12-47) of each GTPCHI at the N-terminus were not defined in the current electron density map, probably due to disorder. However, it has been suggested that this region have little effect on the activity of this enzyme [Auerbach, *et al.*, 2000]. It has also been suggested that the N-terminal region play only a small role in feedback regulation by GFRP [Yoneyama *et al.*, 1997; Auerbach, *et al.*, 2000].

The stimulatory GTPCHI-GFRP complex consists of three layers, $(GFRP)_5$-$(GTPCHI)_{10}$-$(GFRP)_5$, with overall dimensions of approximately 130-Å height and 93-Å diameter (Fig. 4-1a). GFRP forms a pentamer that is arranged as a compact ring (with a 56-Å diameter and a 32-Å height), as suggested by a previous study using gel filtration [Yoneyama & Hatakeyama, 1998]. The GTPCHI decamer consists of two homo-pentameric rings and forms a torus-shaped

structure with dimensions of 93-Å in diameter and 66-Å in height. Two GFRP pentamers interact with top and bottom molecular surfaces of the torus-shaped GTPCHI decamer, sharing the same five-fold axis. At each interface between GFRP and GTPCHI, five phenylalanine molecules are located (Fig. 4-1b). This binding stoichiometry of phenylalanine is consistent with that determined by the equilibration gel filtration method by Hummel and Dreyer [Yoneyama & Hatakeyama, 2001]. Each active site of the GTPCHI monomer contains one zinc ion (Fig. 4-1b).

The overall structure of the inhibitory complex is almost the same structure as that of the stimulatory complex (Fig. 4-1b); two GFRP pentameric rings are docked top and bottom surfaces of the GTPCHI decamer. The height of the inhibitory complex (129.5 Å) was little shorter than that of the stimulatory complex (130.3 Å), this may be occurred by conformational changes with allosteric regulation discussed in the later part of this paper.

The N-terminal regions of GTPCHI (residues 12-47) were also disordered in all ten subunits. While the loop region of residues 206-214 of GTPCHI was disordered in the zinc-depleted inhibitory complex (data not shown), an electron density was seen at this region. The GTP binding to the inhibitory complex may contribute to

stabilize this loop. In fact, the GTP-binding rate in the zinc-carrying inhibitory complex is higher than in the zinc-depleted inhibitory complex (Hatakeyama, personal communication). In fact, Arg^{207} located at this loop is involved in GTP binding [Nar *et al.*, 1995]. The electron densities of BH_2 molecules were clearly observed at the interface between GTPCHI and GFRP in the initial Fo-Fc map, with the deoxy-GTP was not observed except the triphosphate portion at GTP the binding site (Fig.4-15).

4-2. GTPCHI Structure

Both of the rat GTPCHI monomer structures in the stimulatory complex (rsGTPCHI) and the inhibitory (riGTPCHI) complex are basically the same as that of the N-terminal-deleted human GTPCHI (hGTPCHI) [Auerbach *et al.*, 2000] or *E. coli* GTPCHI (eGTPCHI) [Nar et al., 1995b](Fig. 4-2,4-3a). The rms deviations of C^{α} atoms of the whole GTPCHI subunit are, 1.30 Å (rsGTPCHI vs riGTPCHI), 2.55 Å (eGTPCHI vs riGTPCHI), 1.05 Å (hGTPCHI vs riGTPCHI), 0.91 Å (hGTPCHI vs rsGTPCHI) and 2.46 Å (eGTPCHI vs rsGTPCHI). The large deviations are observed in loop αd-β1 and loop αg-β4 (Fig.4-3b). Comparing the rmsd values, the hGTPCHI structure, which is the GFRP-free form of mammalian GTPCHI, resembles to the stimulatory

form of GTPCHI rather than that of the inhibitory form.

The decameric structure of GTPCHI has a β-barrel core in central region (Fig. 1-4). This β-barrel core is consisted of four anti-parallel β-sheets from one subunit. The rms deviations of C^{α} backbone atom at these four β-sheets region are, 0.39 Å (rsGTPCHI vs riGTPCHI), 0.50 Å (eGTPCHI vs riGTPCHI), 0.38 Å (hGTPCHI vs riGTPCHI), 0.25 Å (hGTPCHI vs rsGTPCHI) and 0.45 Å (eGTPCHI vs rsGTPCHI), respectively.

4-3. GFRP Structure

The GFRP monomer consists of a six-stranded antiparallel β-sheet and two α-helices. These secondary structure elements are arranged into a ββαββαββ topology, which could belong to the (α+β) protein class in the SCOP classification [Murzin *et al.*, 1995] (Fig. 4-5). A DALI [Holm & Sander, 1993] search reveals the highest structural similarity with a Z score of 3.8 for a yeast protein YciH [Cort *et al.*, 1999], which is a product from a structural genomic project and the function of which remains unknown. YciH lacks a β-strand corresponding to the C-terminal strand of GFRP (Fig. 4-5).

At the centre of the loop β1-β2 (residues 9-14) of GFRP, the

electron density for a possible metal ion is found. Judging from the coordination, the thermal factor value and the contents of crystallization solvent, it was assumed as a potassium ion. The backbone carbonyl groups of Gln^{9}, Arg^{11}, Val^{14}, Gly^{15} and the side-chain oxygen atom of Thr^{8} are trapping the potassium ion (Fig. 4-6). In the inhibitory complex, the trapped ion was assumed as sodium ion based on the contents of crystallization solvent at the same position as stimulatory complex.

4-4. Structural Similarity between the GFRP Pentamer and the β-propeller Structure

GFRP forms a pentamer in physiological conditions [Yoneyama *et al.*, 1997]. In our pentameric structure, three β-sheets (β5, β6 and β1) of each subunit are arranged radially to form an unique propeller structure (Fig. 4-7a). The interactions between two adjacent GFRP subunits are mainly the hydrophobic interaction, while two hydrogen bonding interactions are observed between Arg^{11} N^{η} and Glu^{46} O^{γ}, and between Arg^{54} N^{ε} atom and Asp^{21} O^{δ} atom.

Interestingly, the architecture of the GFRP pentameric ring is very similar to the β-propeller domains found in several proteins, such as Crathlin heavy chain [ter Haar *et al.*, 1998], Tup1 [Sprague

et al., 2000] and G- subunit [Sondek *et al.*, 1996] (Fig. 4-8, right), containing characteristic sequence repeats of about 50 residues in a single polypeptide chain [Fülöp & Jones, 1999]. To date, β-propeller structures with a 4-, 6-, 7- and 8-fold propeller geometry have been found in functionally unrelated proteins. Recently, a five-fold β-propeller has been found in a lectin, Tachylectin-2 [Beisel *et al.*, 1999] (Fig. 4-8, middle).

Each GFRP monomer corresponds to a blade of the propeller, which is formed by each repeat in the classical β-propeller protein. The buried-tryptophan residue in a non-polar environment, which is one of the particular features of β-propeller structures, is also observed at Trp^{79} (Fig. 4-8). Thus, in contrast to these proteins that have blades in a single polypeptide chain, GFRP provides the first example of a homo-oligomeric β-propeller structure.

The GFRP pentamer exhibits several remarkable features distinct from those of β-propeller proteins. As is the case with β-propeller proteins, the main forces that form the GFRP pentamer seem to be mediated by hydrophobic interactions at the inter-subunit interfaces, which involve several non-polar residues of the innermost, second and third β-strands (Fig 4-9a). However, the

inter-subunit interactions in the GFRP pentamer seem to be much stronger than those of inter-blade interactions of β-propeller proteins. The total buried accessible surface area for the GFRP monomer is 2190 $Å^2$, which is larger than that of other β-propeller proteins (for example, 1530 $Å^2$ for one repeat of Tachylectin-2). Moreover, the GFRP pentamer has the unique interactions among the central β-strands, which pack together around the central 5-fold axis without main chain-main chain interaction to form an inter-subunit β-sheet. In particular, the side chains of Ser^{69} and Thr^{71} play key roles in intimate side-by-side interactions between each pair of β5 strands, thus forming inter-strand hydrogen bonds (Fig. 4-8c,d,e).

GFRP contains no sequence motif similar to the WD repeat [Smith *et al.*, 1999], nor the kelch repeat [Adams *et al.*, 2000], both of which are popular repeats for β-propeller structures. In addition, the β-sheet topology of GFRP is different from those of the β-propeller proteins. The anti-parallel β-sheets of the β-propeller proteins are formed sequentially with the N-terminal β-strand being located at the centre of the propeller, that is, β1-β2-β3-β4 from the inside to the outside of the β-propeller. In contrast, the anti-parallel β-sheet arrangement of GFRP is

β5-β6-β1-β2 from the inside to the outside (Fig. 4-9a). Nevertheless, superposition of the inner three β-strands between GFRP and Tachylectin-2 results in a relatively small value of the root-mean-square deviation for C^{α} carbon atoms (0.78 Å) (Fig. 4-9b). In GFRP, two helices and an anti-parallel β-sheet (β3-β4) are inserted between β2 and β5 strands (Fig. 4-4). This inserted β-sheet protrudes the connecting loop (loop β3-β4) toward the bound GTPCHI.

4-5. Phenylalanine-Binding Site

In our stimulatory complex, five L-phenylalanine molecules are located at the inner regions of the GTPCHI-GFRP interfaces (Fig. 4-1b) and are completely buried inside the interfaces. The total buried accessible surface area of each GFRP-GTPCHI interface, including these trapped five phenylalanine molecules, is increased to 6002 $Å^2$, which is significantly larger than that (3726 $Å^2$) without the phenylalanine molecules. Thus, phenylalanine binding enhances the association of GFRP with GTPCHI by occupying the spaces at the interfaces to increase the contact area. The GFRP pentamer forms five phenylalanine-binding cavities to accommodate the phenyl group (Fig. 4-10c), while the GTPCHI decamer has no such cavity for phenylalanine (Fig. 4-10a). Recent ligand binding studies using

equilibration gel filtration [Yoneyama & Hatakeyama, 2001] have indicated that phenylalanine weakly binds free GFRP, but not free GTPCHI. These observations are consistent with our structure, in which the phenylalanine-binding cavity is primarily located on GFRP rather than on GTPCHI. Each binding cavity on the GFRP pentamer is located at each inter-subunit region between two adjacent subunits and consists of loops β1-β2 and β5-β6 from one GFRP monomer, and loop β5-β6 from the adjacent monomer. Thus, loop β5-β6 participates in the recognition of two phenylalanine molecules on both sides, although no significant cooperativity of phenylalanine-binding has been observed [Yoneyama & Hatakeyama, 2001]. We have found a tentative potassium ion trapped inside the loop β1-β2, of which conformation seems to be stabilized by the bound potassium ion, whereas the ion has no direct interaction with the bound phenylalanine (Fig. 4-6,4-10b).

The phenylalanine-binding cavity is tiled with hydrophobic residues, which interact with the hydrophobic phenyl group of the bound phenylalanine (Fig. 4-10d,e). The amino and carboxyl groups of phenylalanine form six hydrogen bonds with GFRP. Two GFRP residues, Gln^{75} and Gln^{9}, participate in the hydrogen-bonding interactions through their side chains: the side chain of Gln^{75} from

one GFRP subunit is directly hydrogen-bonded with the amino and carboxyl groups of phenylalanine; the side chain of Gln^{9} from the other GFRP subunit forms a water-mediated hydrogen bond with the amino group. This water molecule is also linked to the side chain of Glu^{227} from GTPCHI and the main-chain carbonyl group of this GTPCHI residue forms a direct hydrogen bond with the amino group of the bound phenylalanine. Thus, Glu^{227} is a single key residue from GTPCHI involved in the recognition of phenylalanine.

4-6. BH_2-Binding Site

BH_4 (or BH_2) is an essential substrate for formation of the inhibitory complex [Harada *et al.*, 1993; Yoneyama & Hatakeyama, 1998]. In our crystal structure, ten BH_2 molecules were found in the GTPCHI-GFRP interfaces (Fig. 4-1b). These BH_2 molecules are found to interact with GTPCHI rather than GFRP. This is coincident with previous results for investigating of BH_4 binding site using Hummel & Drayer method [Yoneyama & Hatakeyama, 2001]. The BH_2-binding site consists of two-neighbouring GTPCHI subunits; residues 220-231 from one chain and residues 118-120, 148-150 and 224-234 from another chain (Fig. 4-11b,c). Many acidic residues, such as Asp^{118}, Asp^{228} and Glu^{234} exist at the BH_2-binding cavity to

interact the basic BH_2. Two water molecules were found to mediate hydrogen bonds to BH_2. Moreover, Arg^{232} stacks on the pterin ring together with two residues of Leu^{148} and Val^{224}. While the aromatic ring of BH_2 interacts with many GTPCHI residues (Fig. 4-11b), the side chain from the ring has no interaction with GTPCHI and weak van der Waals contacts (3.5 Å) with Gln^{9} from GFRP.

4-7. GTPCHI-GFRP Interaction

Three GFRP loops, loops β1-β2 (residues 9-16), β3-β4 (residues 38-45), and β5-β6 (residues 73-75), make contact with GTPCHI (Fig. 4-4,4-10a). Loop β3-β4 from the inserted β-sheet contacts one GTPCHI subunit at the outer region of the interfaces between GFRP and GTPCHI, while loops β1-β2 and β5-β6 contact the other adjacent GTPCHI subunit at the innermost region of the interfaces. Thus, one GFRP monomer makes contact with two GTPCHI subunits (Fig. 4-10b).

At the innermost regions of the interfaces close to the five-fold axis (Fig. 4-12), Ile^{10} and Arg^{11} from loop β1-β2 and Gln^{75} from loop β5-β6 make contact with the GTPCHI residues 227-230 of the N-terminal region of the C-terminal helix. These contacts involve van der Waals interactions and a salt bridge formed between

Arg^{11} from GFRP and Glu^{227} from GTPCHI (Fig. 4-10d).

At the outermost region of the interfaces of the stimulatory complex (Fig. 4-13a), Asn^{42} from GFRP loop β3-β4 forms direct and also water-mediated hydrogen bonds with Glu^{227} and Arg^{226} from GTPCHI, respectively. In addition, two nonpolar GFRP residues Leu^{40} and Gly^{41} from loop β3-β4 make hydrophobic interactions with Val^{182} and Leu^{222} from GTPCHI, respectively. In the inhibitory complex (Fig. 4-13b), the backbone carboxyl group of Leu^{40} of GFRP interacts with Gly^{223} of GTPCHI through a water molecule. As the results of BH_2-binding, the side chains of Arg^{226} and Glu^{227} are shifted and loose the interactions observed in the stimulatory complex. Moreover, the side chain of Asn^{43} of GFRP is also altered in the inhibitory complex to form novel hydrogen bonds with the backbone carboxyl groups of Gln^{189} and Pro^{190} (Fig. 4-13).

4-8. Active Site

The active site of GTPCHI is located at the interface of three GTPCHI subunits: two neighbouring subunits (A and B) and one from opposite pentameric ring (C). The active site consists of residue 130-137, 169-177 and 200-208 of chain A, residues 112-114 and 153-162 of chain B and residues 84-91 of chain C (Fig. 4-2). The

zinc ion is thought necessary to initiate the ring-opening reaction of GTP substrate catalysed by GTPCHI [Auerbach *et al.*, 2000].

In this crystallographic study, the zinc ion liganded to Cys^{132}, His^{134} and Cys^{203} (Fig. 4-14) is found in both the inhibitory and stimulatory complexes. The average distances between the zinc atom and the Cys^{132} S^{γ} atom, the His^{134} N^{δ} atom and the Cys^{203} S^{γ} atom are 2.22 ± 0.07 (inhibitory: 2.37 ± 0.07) Å, 2.16 ± 0.05 (2.30 ± 0.05) Å and 2.37 ± 0.08 (2.48 ± 0.07) Å, respectively. Superimposition of the zinc ions and the ligands in the GTPCHI structures revealed that there are no significant positional changes at these residues and the zinc atom in rsGTPCHI, riGTPCHI, hGTPCHI and eGTPCHI (Fig. 4-14).

In the inhibitory complex, the GTP molecule is essential for the complex formation [Harada *et al.*, 1993; Yoneyama & Hatakeyama, 1998]. In the crystal structure of the inhibitory complex, only the triphosphate moiety of deoxy-GTP was defined at active site (Fig. 4-15). The electron density of the triphosphate is relatively clear at the γ-site rather than the α-site. There are poor electron densities for the guanosine moiety of deoxy-GTP.

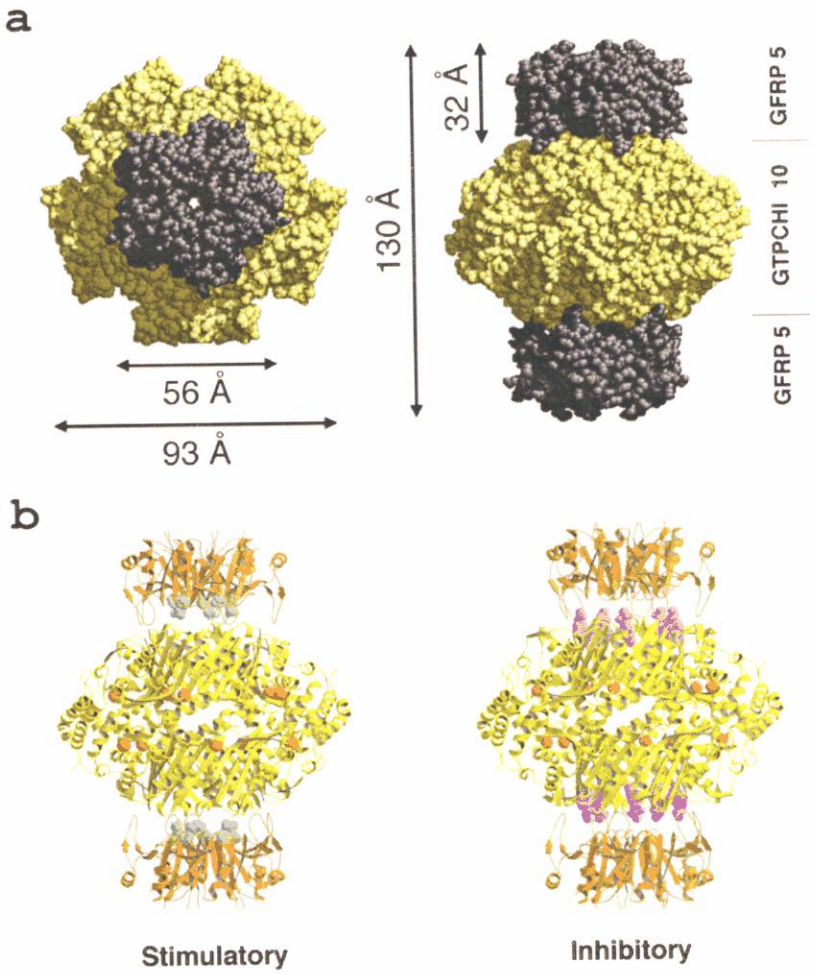

Figure 4-1. Overall structures of the GTOCHI-GFRP complex. (a) Space-filled representation of the stimulatory complex. GTPCHI and GFRP are coloured with amber and black, respectively. (b) Ribbon representation of the stimulatory (left) and the inhibitory (right) complexes. GTPCHI and GFRP subunits are coloured in amber and orange, respectively. The zinc ions at the active sites are indicated as red spheres. The ligand molecules of the stimulatory (Phe, cyan) and the inhibitory (BH_2, pink) are shown as space-filled models.

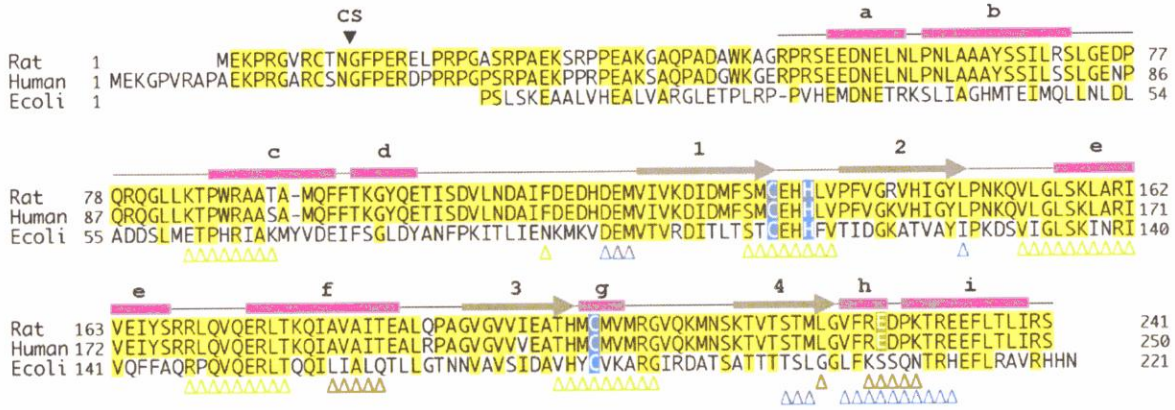

Figure 4-2. Sequence alignment of rat, human and *E. coli* GTPCHI. The identical residues are highlighted in yellow. The secondary structure symbols (α-helices (magenta rectangles) and β-strands (grey arrows)), which were determined in this study, are indicated above the sequence. The cleavage site observed in rat-liver-derived GTPCHI is indicated (CS) [Hatakeyama *et al.*, 1989]. Thus, the N-terminal of the mature form of rat GTPCHI starts with Gly-Phe-Pro-, and the mature form was used in the structural study. The residues participates in zinc binding are highlighted in blue. Glu^{227} involved in phenylalanine interaction is highlighted in green. The residues located at the active site (Δ), the GFRP interface (Δ) and the BH_2-binding site (Δ) are indicated.

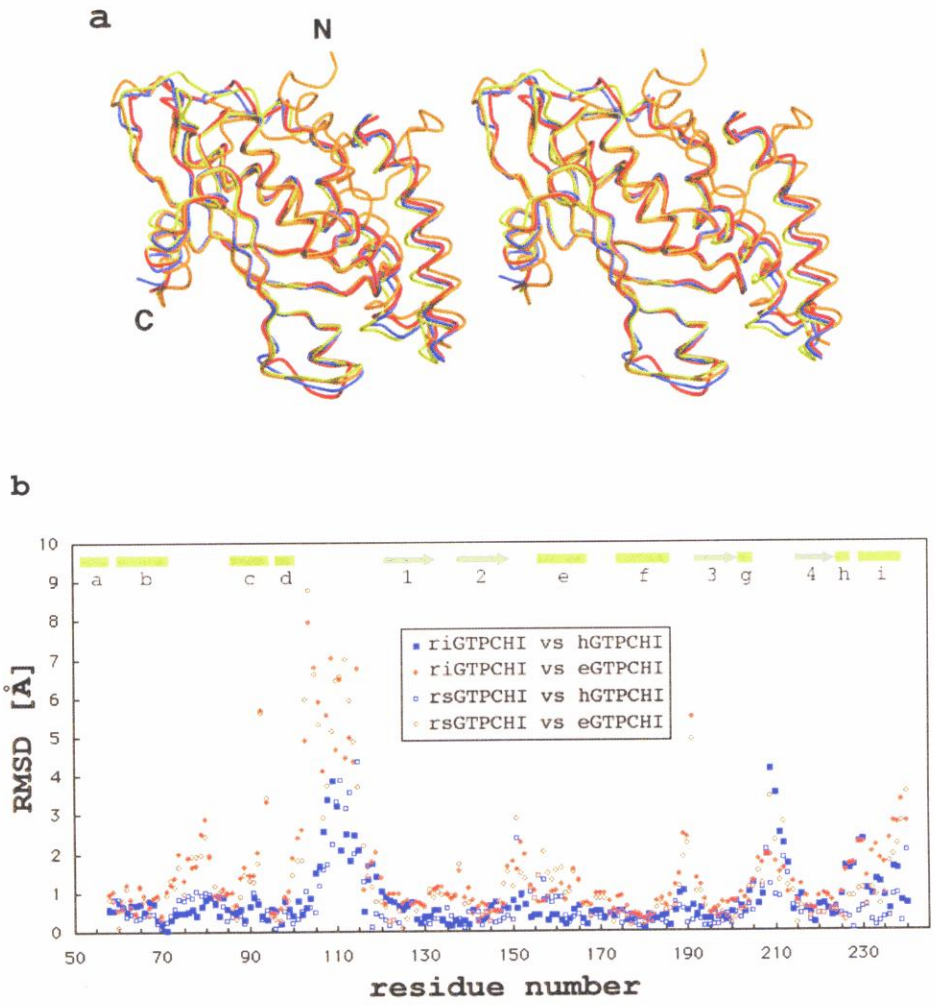

Figure 4-3. Comparison of GTPCHI structures. (a) Stereo view of superimposition of C^{α} carbon atom tracing of rsGTPCHI (red), riGTPCHI (green), hGTPCHI (blue) and eGTPCHI (orange). (b) The positional differences of C^{α} atoms in hGTPCHI and eGTPCHI from those in rsGTPCHI or riGTPCHI are plotted against the residue number.

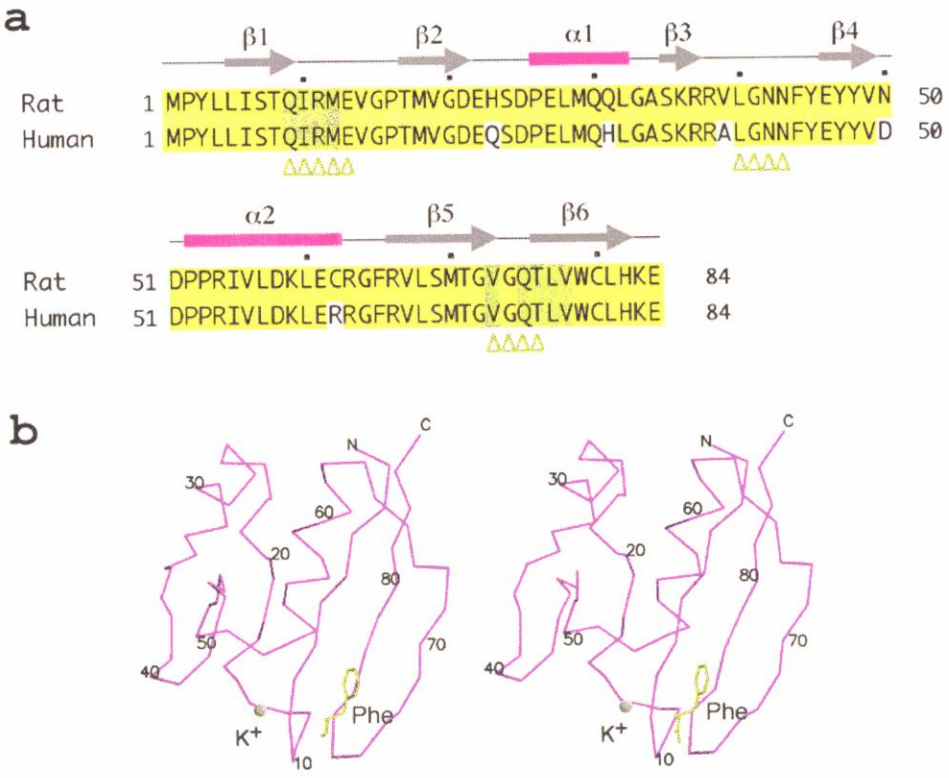

Figure 4-4. (a) The secondary structure elements of the rat GFRP monomer and amino acid sequence alignment of rat and human GFRPs. Identical residues are marked in yellow. GFRP contains two α-helices (pink rectangles) and six β-strands (grey arrows). The residues involved in phenylalanine-binding are coloured in green. The residues located at the GTPCHI contact area are marked with Δ. (b) A stereo view of C^{α} carbon tracing of the GFRP monomer in the stimulatory complex with residues numbers in every tenth residue. The trapped potassium ion is indicated as cyan sphere. The ligand phenylalanine molecule is also indicated as a green stick model.

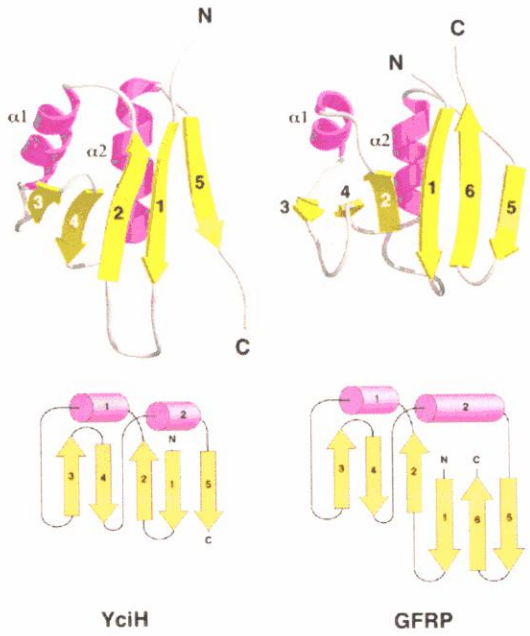

Figure 4-5. Structural comparison of YciH and GFRP. YciH has a ββαββαβ topology, which shows the highest structural similarity to that of the GFRP monomer.

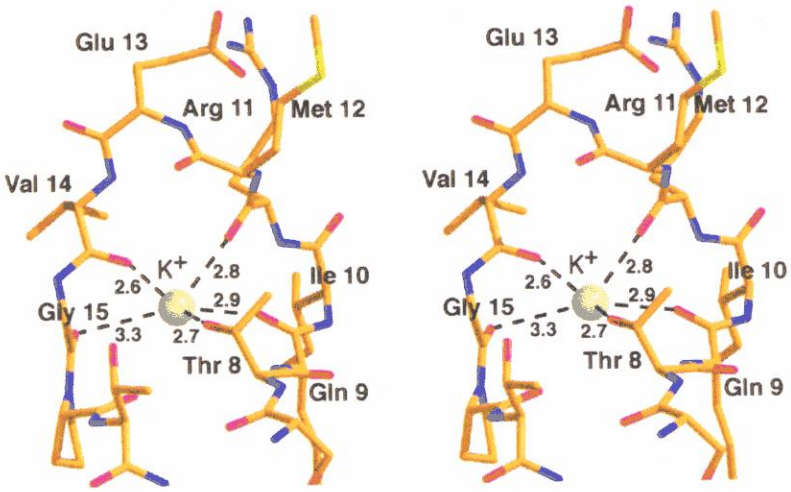

Figure 4-6. Stereo view of the trapped potassium ion at the centre of GFRP loop β1-β2 in the stimulatory complex. The hydrogen bonds are indicated as broken lines. The average distances (Å) in all ten GFRP monomers in the complex are indicated.

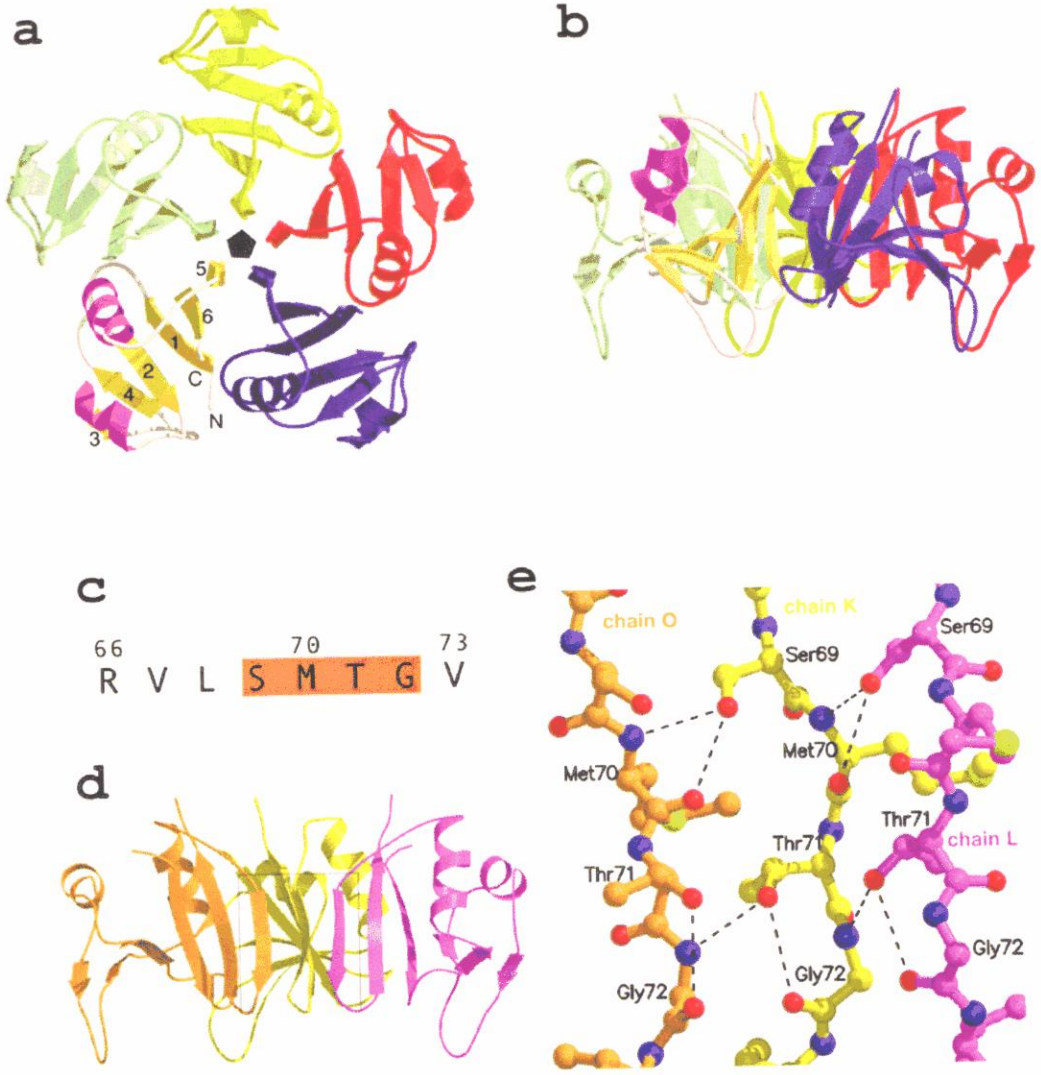

Figure 4-7. GFRP pentameric structure. (a) The GFRP pentamer viewed along five-fold axis. (b) A side-view of the GFRP pentamer. (c)-(e) Subunit-subunit interactions observed in the central β5 strand. The amino-acid sequence of β5 strand (c), a side view of three GFRP subunits (d) with a rectangular box indicating the region shown in (e). A close-up view of the β5 strands of GFRP (e). Broken lines indicate hydrogen bonds involving the side chains of Ser^{69} and Thr^{71}.

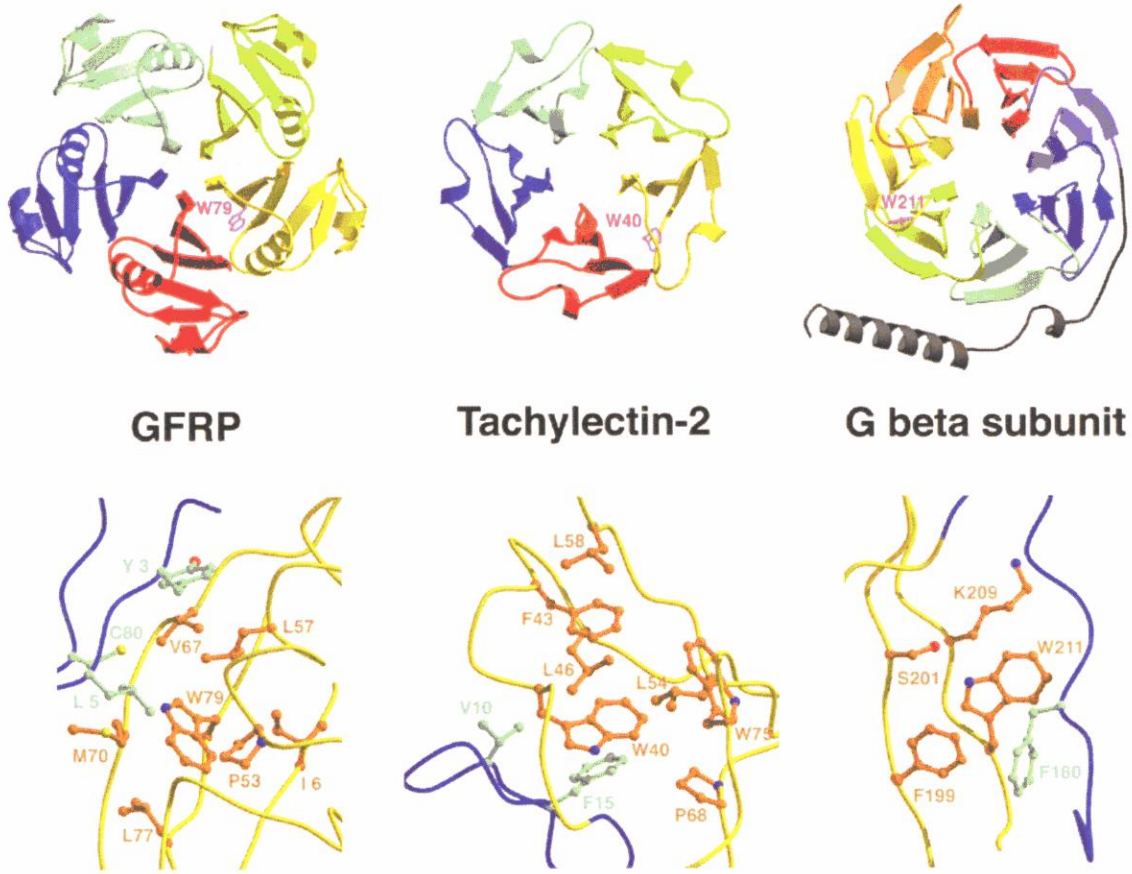

Figure 4-8. A comparison of the GFRP pentamer and β-propeller structures. (top) Views of GFRP (left), Tachylectin-2 (middle), and the hetero-trimeric G protein β subunit (G_β) (right). Each top view is viewed along each 5- (for GFRP and Tachylectin-2) and 7-fold (for G_β) symmetric axis. The five GFRP monomers are shown in different colours. Similarly, each blade of Tachylectin-2 (PDB code 1TL2) and G_β (PDB code 1TBG) is shown in a different colour. (bottom) The tryptophan residue at hydrophobic centre observed in each protein.

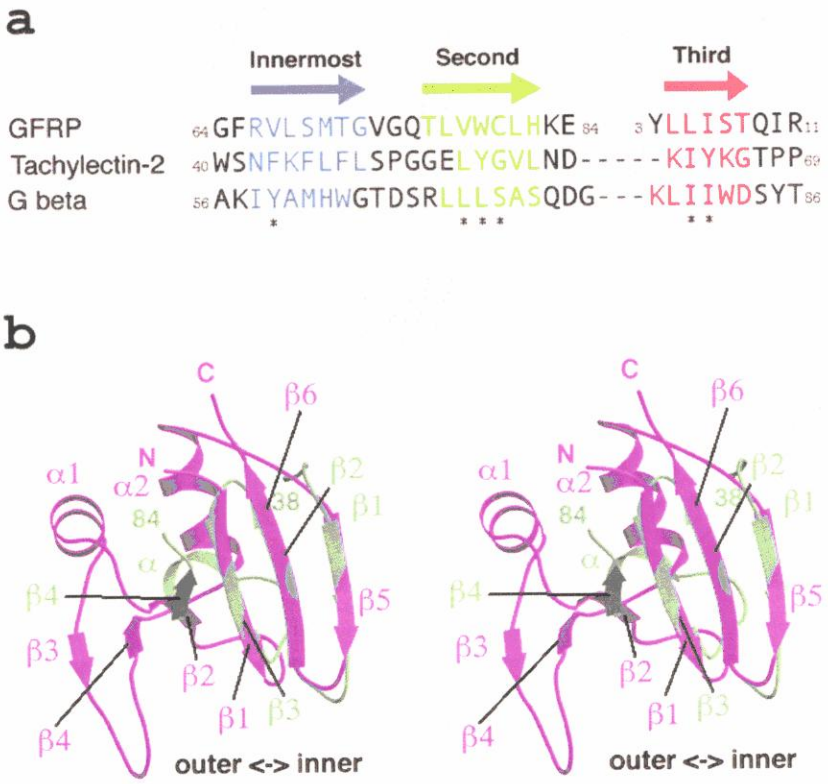

Figure 4-9. (a) Sequence comparison of the inner three β-strands (blue, green, and orange) of the GFRP and β-propeller blades of Tachylectin-2 and the G_{β} subunit. (b) Stereo view of the GFRP subunit (magenta) superimposed onto a blade of Tachylectin-2 (cyan).

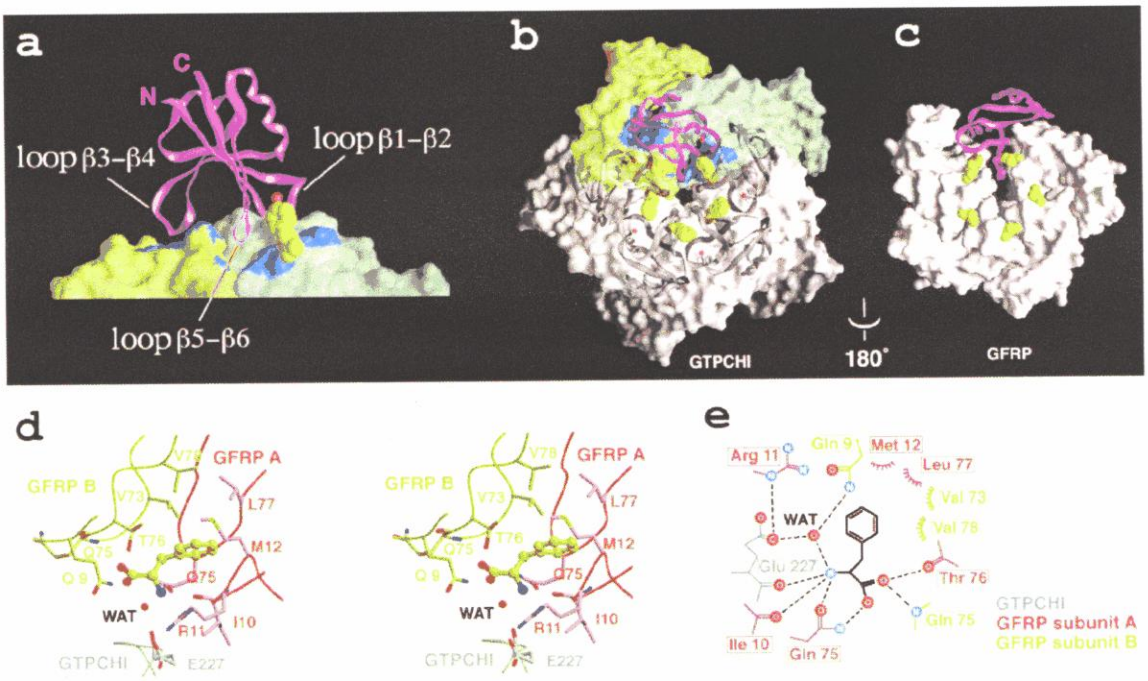

Figure 4-10. The phenylalanine-binding sites at the interfaces between GFRP and GTPCHI. (a and b) The contacts between GFRP and GTPCHI are shown with ribbon models of the GFRP subunits and molecular surfaces of GTPCHI. The panel (a) shows a close-up side view of one GFRP subunit (magenta) that makes contact with two GTPCHI subunits (green and light blue). The panel (b) shows a top-view of the GFRP pentamer on the GTPCHI decamer. In both panels, molecular surfaces coloured in blue indicate the GTPCHI residues contacting GFRP. The bound phenylalanine molecules are shown as space-filled models (yellow). The tentative potassium ions are shown as red balls. (c) Five phenylalanine molecules bound to the stimulatory complex are depicted on the molecular surfaces of the GFRP pentamer with one GFRP monomer as a ribbon model (magenta). The bound phenylalanine molecules are shown as space-filled models (yellow). (d) A close-up stereo view of the phenylalanine-binding site located at the interfaces formed by two GFRP subunits (red and pale green) and one GTPCHI subunit (blue). The bound phenylalanine molecule is shown as a ball-and-stick model (yellow). The bridging water molecule is shown as a red ball with a label (WAT). (e) Schematic representation of the GFRP- and GTPCHI-phenylalanine interactions. Broken lines indicate hydrogen bonds. The two GFRP subunits are coloured in red and pale green, and one GTPCHI subunit in blue. The bound phenylalanine molecule is shown in black lines. The bridging water molecule is labelled with WAT.

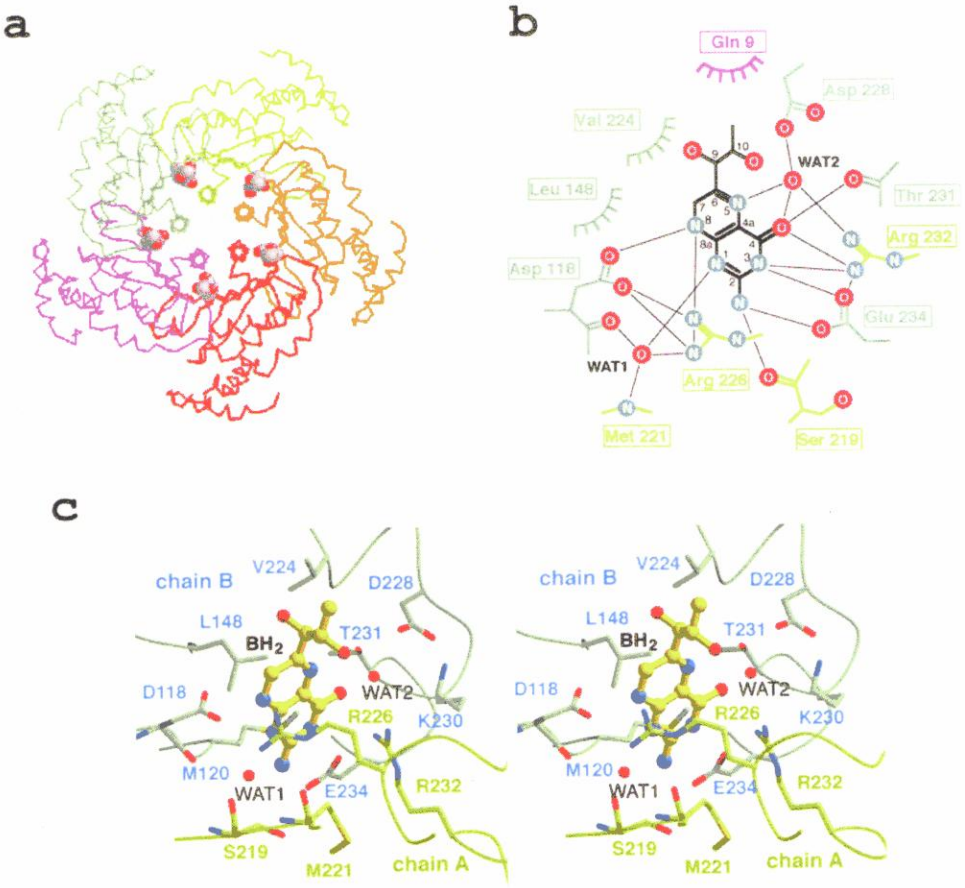

Figure 4-11. (a) A top view of the GTPCHI pentamer of the inhibitory complex. Each subunits are shown as C^{α} backbone tracing representation in different colours. The BH_2 molecules are shown in space-filled models. (b) Schematic drawing of the interactions between BH_2 and protein. The residues from different chains are in different colours. The hydrogen bonds are denoted as thin black lines. (c) Stereo view of BH_2-binding site. The BH_2 molecule is drawn as a ball-and-stick model. The BH_2-binding site is located at the interface of two GTPCHI subunits, chain A (green) and B (cyan). Two water molecules involved in BH_2-binding are also shown with labels (WAT).

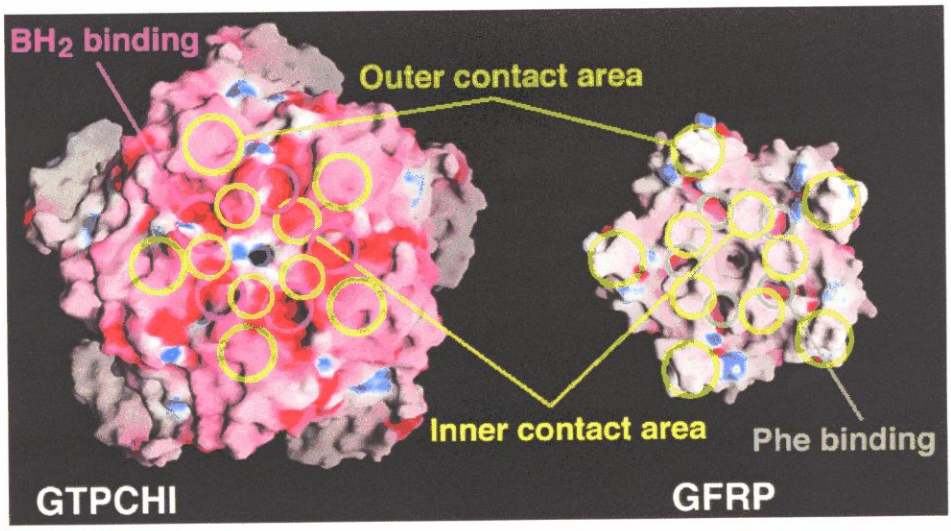

Figure 4-12. Molecular surface and electrostatic potentials of stimulatory GTPCHI (left) and stimulatory GFRP (right) viewed from interacted side. Positive charges are shown in red, negative charges in blue. The ligand-binding sites and contact area of GTPCHI and GFRP pentamer revealed in this study are indicated.

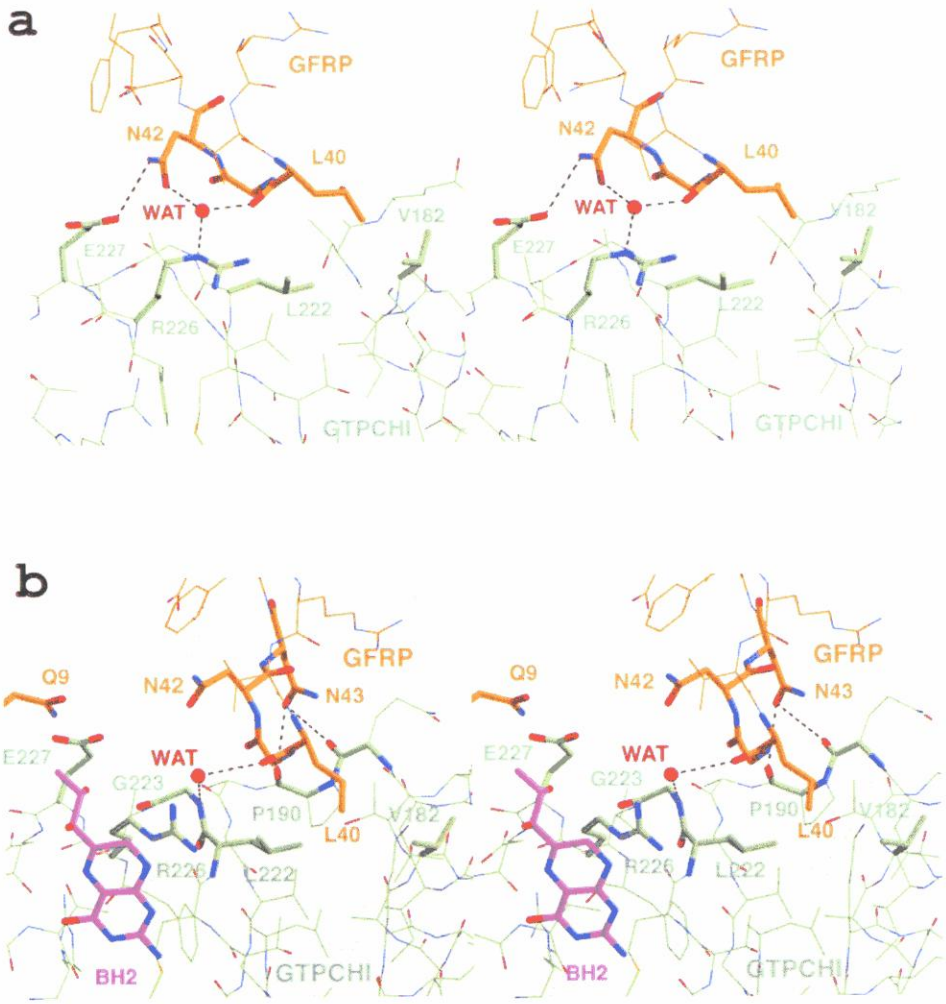

Figure 4-13. Close-up stereo views of the outer GTPCHI-GFRP contact site in the stimulatory (a) and the inhibitory (b) complex. The hydrophobic interactions between Leu^{40} of GFRP and Leu^{222} and Val^{182} of GTPCHI are observed in both complexes. In addition, water-mediated hydrogen bonds involving Gly^{41}, Asn^{42} of GFRP and Arg^{226} (stimulatory) or Gly^{223} (inhibitory) of GTPCHI are observed. In the stimulatory complex, the hydrogen bond between side chains of Asn^{42} of GFRP and Glu^{227} of GTPCHI is found. In the inhibitory complex, there are hydrogen bonds between GFRP Asn^{43} and the carbonyl group of GTPCHI Gln^{189} and Pro^{190}.

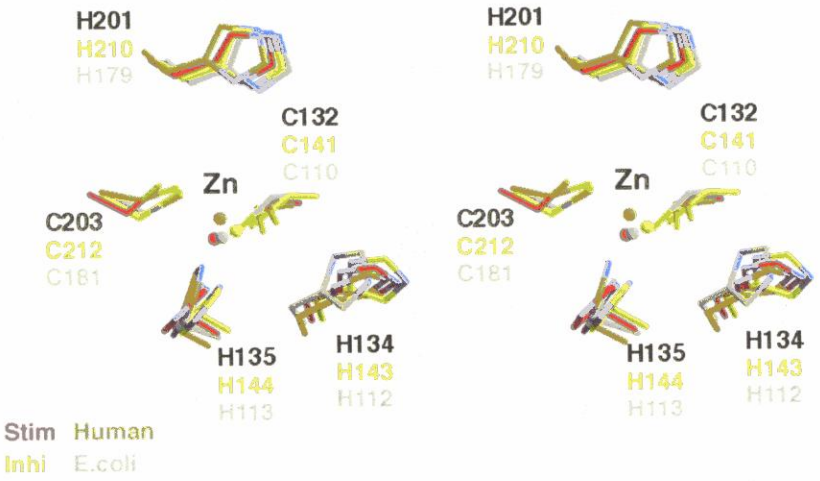

Figure 4-14. A stereo view of superimposed residues (Cys^{132}, His^{134}, His^{135}, His^{201} and Cys^{203}) and zinc ions at the active sites in different GTPCHI structures of GTPCHI. Each colour indicates red for the Rat-stimulatory, green for the rat-inhibitory, orange for the human and cyan for *E.coli* GTPCHI.

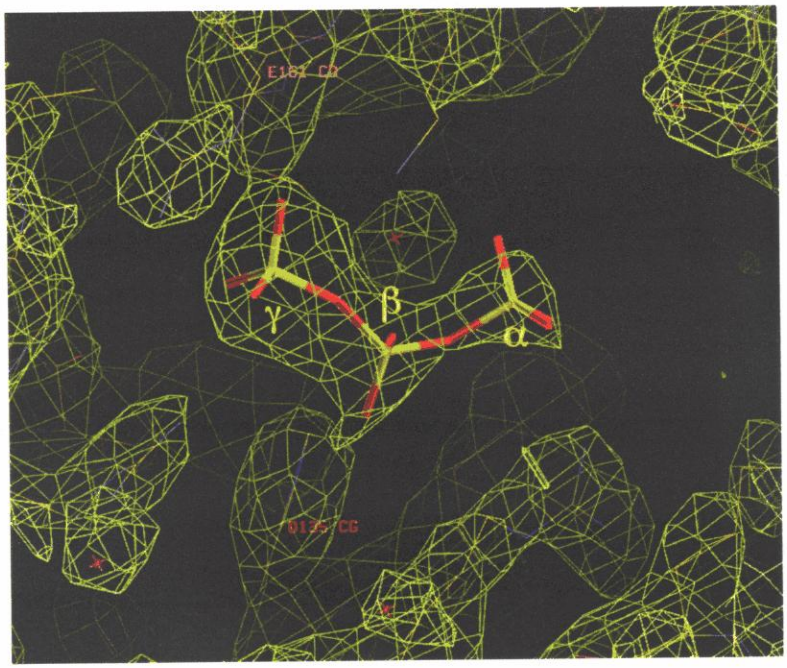

Figure 4-15. Close-up view of the electron density around the triphosphate moiety of deoxy-GTP in the inhibitory complex. The electron density was contoured at 1σ.

Comparison of the GTPCHI-GFRP Stimulatory and Inhibitory Complexes

5-1. GTPCHI and GFRP subunit

Comparing two GTPCHI structures in the stimulatory and inhibitory complexes, conformational changes (rmsd of C^{α} > 1 Å) were observed at five regions; loop αb-αc (residues 79-81), loop αd-β1 (106-121), loop β2-αe (151-157), loop αg-β4 (204-212) and αh-αi (221-234) (Fig. 5-1). Loop αb-αc is involved in triphosphate binding of dGTP in the inhibitory complex. Loop αd-β1, which shows significant conformational changes, forms part of the GTP-binding site and followed by residues 115-121 participating in BH_2-binding. Loop β2-αe contacts residues 115-121 these. Loop αg-β4, which is also involved in GTP-binding, exhibits large conformational changes. In the decameric GTPCHI structure, this loop contacts the corresponding loop of another GTPCHI subunit from the opposite GTPCHI ring. Therefore, conformational changes observed at this region may be linked to quaternary geometrical changes of the GTPCHI decamers. Loop αh-αi is the main component of the BH_2-binding site (Fig. 4-2).

The pentameric GFRP structures are highly conserved in the stimulatory and the inhibitory complexes (average rms deviation of C^{α} carbon atoms is 0.64 Å, at residues 2-83). However, a large local conformational change is found in loop β3-β4 (residues 38-44), which contacts GTPCHI (Fig. 5-2).

As shown in figure 5-2, loop β3-β4 in the inhibitory complex slightly shifts toward inside of the pentameric ring. Interestingly, there is no large change observed in loops β1-β2 and β5-β6, which consist of the phenylalanine-binding site. The recently determined structure of a free form of GFRP [Bader *et al.*, 2001] resembles to that in the inhibitory complex rather than that in the stimulatory complex. The rms displacement values of GFRP C^{α} carbon atoms (residues 2-83) in the free form, the stimulatory and inhibitory complexes are summarized in table 5-1. In the free form of GFRP, Ile^{10} residue is flipped toward the hydrophobic cavity, which is occupied with the aromatic moiety of phenylalanine in the stimulatory complex.

In contrast to small and local structural changes in the GFRP structures in the stimulatory and inhibitory complexes, large structural changes were found in the quaternary structures of the GTPCHI decamer. As shown in figure 5-3a, the central cavity of GTPCHI

is narrowed in the inhibitory complex primarily as a result of changes in interactions between subunits at the centre of the ring. In the stimulatory complex, Glu^{233} and Lys^{230} from each subunit form a hydrogen bond network at the ring centre. In the inhibitory complex, however, the side chain of Lys^{230} flips away from this hydrogen network to make hydrogen bonds with Asp^{228} (Fig. 5-3b). The average distance between adjacent two Lys^{230} N^{ζ} atoms in the rsGTPCHI pentamer is 4.84 ± 0.20 Å, while that for Glu^{233} O^{ε} atoms in the riGTPCHI pentamer is 3.56 ± 0.17 Å.

Superimposition of the inhibitory complex on the stimulatory one so as to yield the maximum overlap between the upper GFRP pentamers, revealed rotations of the GTPCHI pentamer and monomer. The upper GTPCHI pentamers in the inhibitory complex rotate by approximately -4.0° against the upper GTPCHI pentamer in the stimulatory complex. The rotation matrix of one GTPCHI subunit of the upper pentamer is given as

$$GTPCHI_{inhi} = \begin{vmatrix} 0.999 & -0.026 & 0.048 \\ 0.026 & 1.000 & -0.014 \\ -0.048 & 0.015 & 0.999 \end{vmatrix} \times GTPCHI_{stim} + \begin{vmatrix} 0.628 \\ -0.328 \\ 0.139 \end{vmatrix}.$$

This transformation can be divided into two steps. The first step is a -4.0° rotation around the five-fold axis of the complex and the second step is a 3.3° rotation around the axis crossed at the C^{α} carbon atom of Gln^{171} (Fig. 5-3c). This second axis is nearly perpendicular to the five-fold axis. The second rotation results in shrinking of the whole structure in the inhibitory complex than in the stimulatory complex.

5-2. Ligand-Binding Site

As the structural changes between the GFRP structures in the stimulatory and inhibitory complexes are small, the phenylalanine-binding cavity on GFRP was not altered significantly in these complex formations. However, the interactions between phenylalanine and Glu^{227} of GTPCHI should be changed because of the rotation of GTPCHI against GFRP. Superimposition of phenylalanine on the inhibitory complex indicates possible repulsive contacts between the negatively charged carboxyl groups of phenylalanine and GTPCHI Glu^{227} (Fig. 5-4b).

The BH_2-binding site induces local structural changes of GTPCHI including Glu^{233} and Lys^{230} (Fig. 5-5). In the stimulatory complex, Lys^{230}(B) interacts with Glu^{233}(A) and Glu^{233}(B), while

Asp^{288}(B) interacts with Thr^{231}(B). In the inhibitory complex, the side-chain of Glu^{233} orients toward the central cavity. At the same time, the side-chain of Lys^{230}(B) bends upward to interact with Asp^{288}(B). Thr^{231}(B) participates in the BH_2 recognition. In addition, the hydrogen bond between Glu^{119}(B) O^{ε} atom and backbone amino group of Met^{221}(A) in the stimulatory complex is broken and a water molecule replaces the Glu^{119}(B) position in the inhibitory complex (Fig. 5-4a).

Especially, the residues 106-115 have a significant induced fit by the formation of BH_2-binding. The side chain of Asp^{118}(B) re-oriented to interact with BH_2 and Arg^{226}(A), forming the BH_2-binding pocket. These structural changes are propagated to Glu^{119}(B), His^{117} (B) and residues 106-116. As shown in figure 5-6a, the side chain of His^{117}(B) re-orientates and makes a hydrogen bond with Asp^{114}(B) (Fig. 5-6a). The inter-subunit interaction between Arg^{176}(A) and Glu^{115}(B) in the stimulatory complex is broken with these changes. As a result of these changes, the backbone of residues 110-115 shift up by 3.3 Å.

5-3. Active Site

The guanosine-binding site found in the *E. coli* GTPCHI-GTP

complex is formed by five loops to provide a pocket for the aromatic guanine ring [Nar *et al.*, 1995b]. This pocket is also found in the current GTPCHI-GFRP complexes. In the stimulatory complex, two loops from the subunit B (Fig. 5-6a) contain Phe^{113}(B) and Leu^{156}(B), respectively. These two residues are located at positions able to make direct hydrophobic contacts with the postulated guanine ring. Especially, Phe^{113}(B) plays a role as a lid of the pocket (Fig. 5-6). The other three loops came from the subunit A and contain His^{134}(A), Arg^{176}(A) and His^{201}(A), respectively. In the inhibitory complex, the loop containing Phe^{113}(B) is shifted away from the pocket, while another loop containing Leu^{156}(B) moves toward the pocket so as to occupy the pocket space with the Leu^{156}(B) side chain. Therefore, the guanine-binding pocket of the inhibitory complex becomes a shallower one, which is open to the solvent region. These local structural changes are triggered by BH_2-binding, which induces a large shift of the loop containing Phe^{113}(B). Due to these shifts, the GTP binding pocket is open in the inhibitory complex, while it is completely closed in the stimulatory complex, as well as in the active site of eGTPCHI (Fig. 5-6c).

The GTP-binding site found in the *E. coli* GTPCHI-GTP complex is located at the inter-subunit of three GTPCHI subunits; two

neighbouring subunits and one subunit from the opposite GTPCHI pentamer ring. There are five essential residues of Cys^{132} (Cys^{110} in *E. coli*), His^{134} (His^{112}), His^{135} (His^{113}), His^{201} (His^{179}) and Cys^{203} (Cys^{181}) at the active site [Nar *et al.*, 1995b]. All these residues belong to subunit A, not to subunit B. Three of them, Cys^{132}, His^{135} and Cys^{203} bind a zinc ion with tetrahedral geometry and the remainder binds a water molecule that is considered to be activated for the initiation of the guanine ring opening (Fig. 1-2). The zinc ion is considered as an essential ion for enzyme activities, because *E. coli* GTPCHI purified without chelating agents shows five-fold enzyme activities than GTPCHI purified with EDTA [Auerbach *et al.*, 2000]. In hypothetical reaction model, the zinc ion activates the water molecule for the nucleophile attack to the C8 atom of GTP [Auerbach *et al.*, 2000] (Fig. 1-2). In this crystallographic study, I confirmed the zinc ion located at the centre of Cys^{132} S^{γ}, His^{135} N^{δ} and Cys^{203} S^{γ} atoms in the GTPCHI-GFRP complexes. The superimposition of the stimulatory and the inhibitory complexes around the active site revealed that the arrangements of Cys^{132}, His^{134}, His^{135}, His^{201}, Cys^{203} and the zinc ion were almost unchanged (Fig. 4-14).

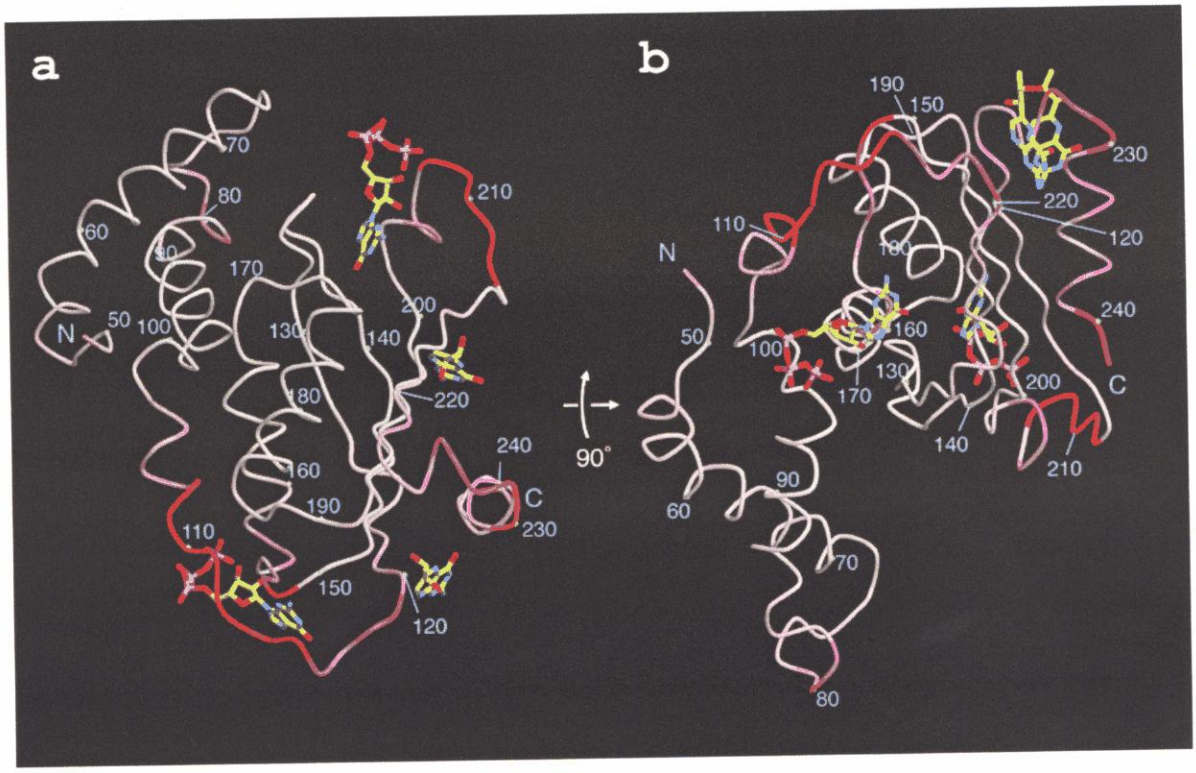

Figure 5-1. Positional differences between C^{α} carbon atoms of riGTPCHI and rsGTPCHI. (a and b) The deviations are mapped as white to red colours on C^{α} traced model of riGTPCHI. A view along the five-fold axis in (a) and is rotated by 90° in (b). The GTP and BH_2 molecules are superimposed to clarify their binding-sites. (c) The deviations and thermal factors are plotted against the residue number.

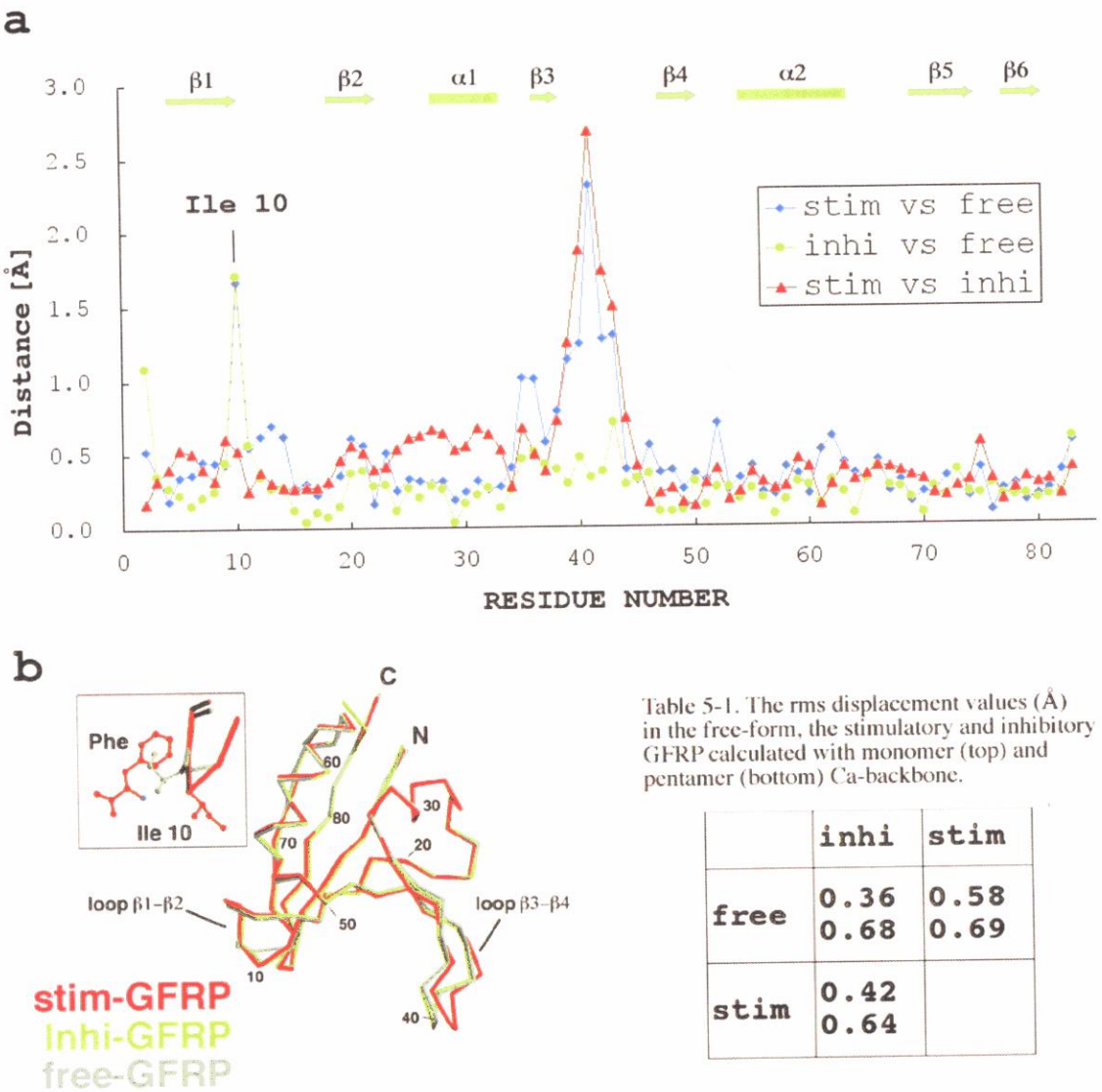

Table 5-1. The rms displacement values (Å) in the free-form, the stimulatory and inhibitory GFRP calculated with monomer (top) and pentamer (bottom) Cα-backbone.

	inhi	stim
free	0.36 0.68	0.58 0.69
stim	0.42 0.64	

Figure 5-2. (a) The distances between corresponding C^{α} atoms of the inhibitory, stimulatory and free-forms of GFRP. The distances are plotted against the residue number. (b) Superimposition of the inhibitory (green), stimulatory (red) and free-form (cyan) of GFRP. A close-up view around the Ile^{10} (phenylalanine binding site) and ligand molecule (Phe) is shown in the box.

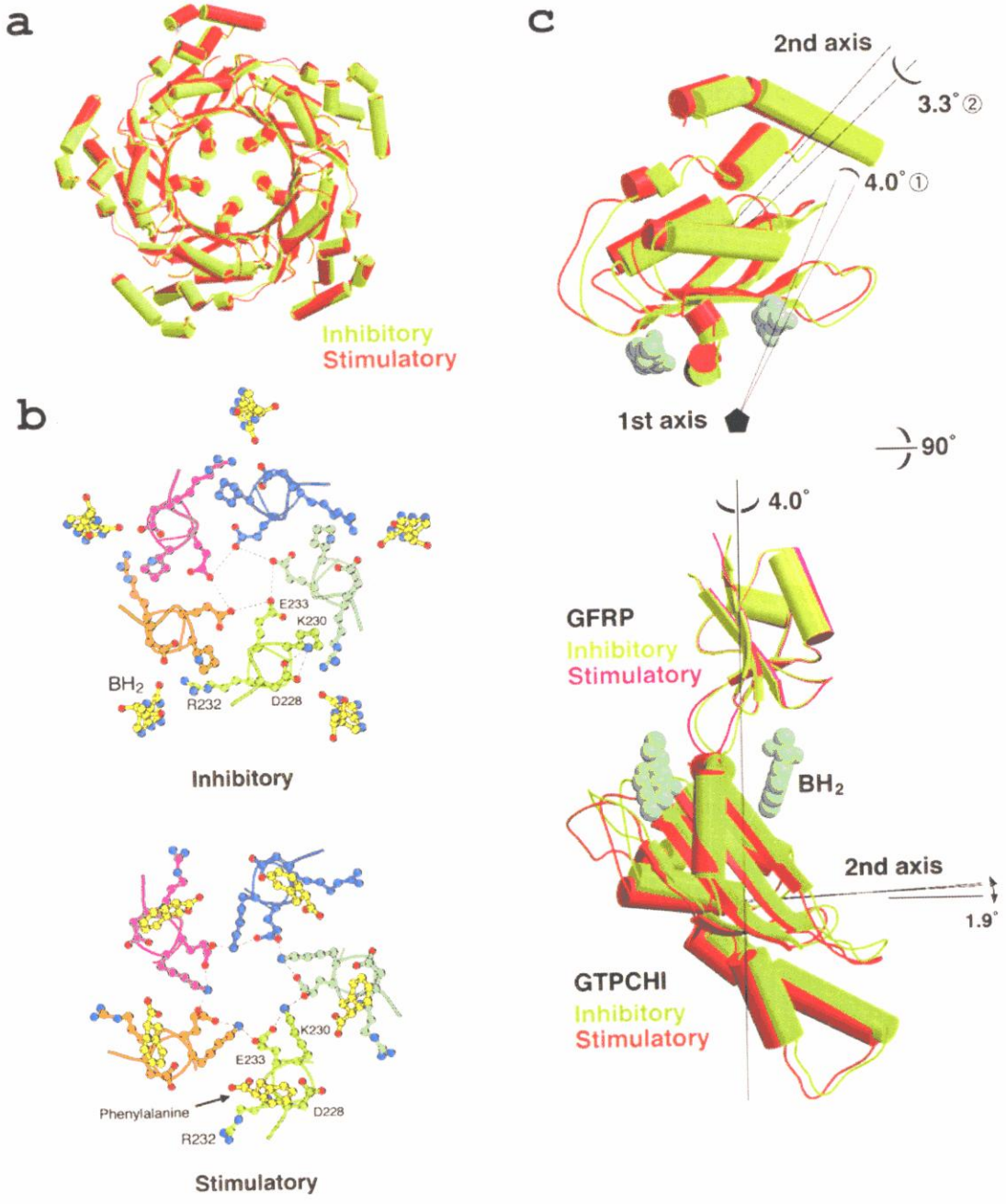

Figure 5-3. (a) Superimposition of the riGTPCHI (green) and the rsGTPCHI (red) pentamer. The fitting calculation was done with C^{α} atoms of inner twenty β-strands. Clearly, the central cavity is narrowed in the inhibitory complex. (b) The inter-subunit interactions in the central cavity. In the stimulatory complex (bottom), the hydrogen-bonding network formed by Glu^{233} and Lys^{230} is indicated by broken lines. (c) Quaternary structural changes between the stimulatory and inhibitory complexes. The fitting

calculation was done between C^{α} atoms of each GFRP. The GTPCHI subunit rotation from the stimulatory to the inhibitory complex is shown as a combination of two rotations (1 and 2). The first rotation is 4.0° about the 5-fold axis. The second rotation is 3.3° about the axis through a C^{α} carbon atom of Gln^{171}.

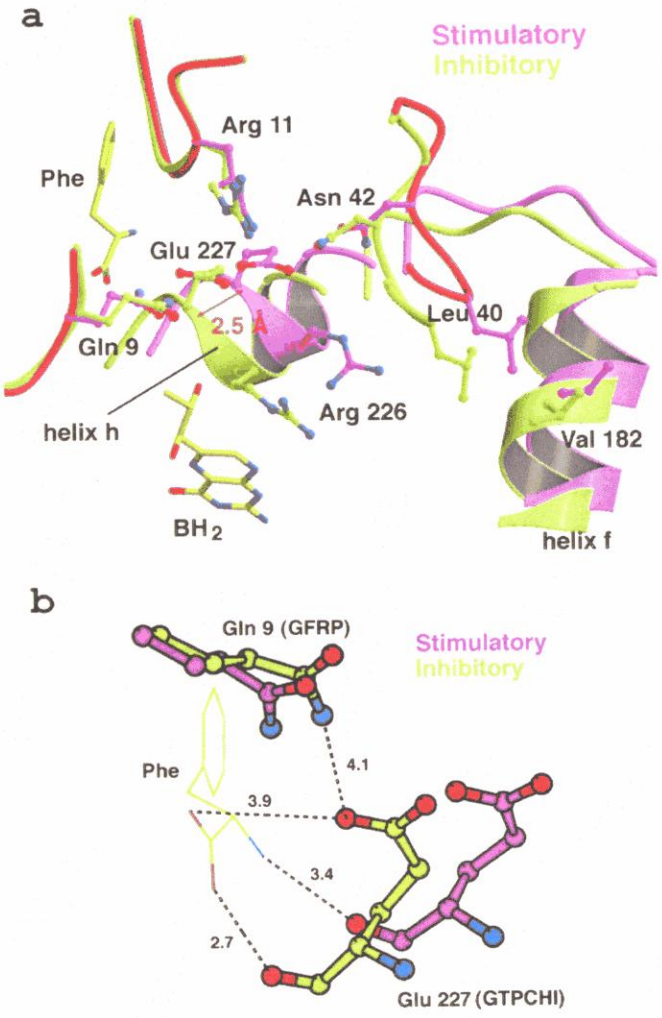

Figure 5-4. (a) Superimposed ligand-binding site in the inhibitory (green) and stimulatory (red) complexes. Compared with the stimulatory complex, helix **h** (224-227) of the inhibitory GTPCHI complex slides about 2.5 Å toward to the central cavity. The ligand molecules (Phe and BH_2) are shown in yellow. (b) Close-up view of the phenylalanine-binding site.

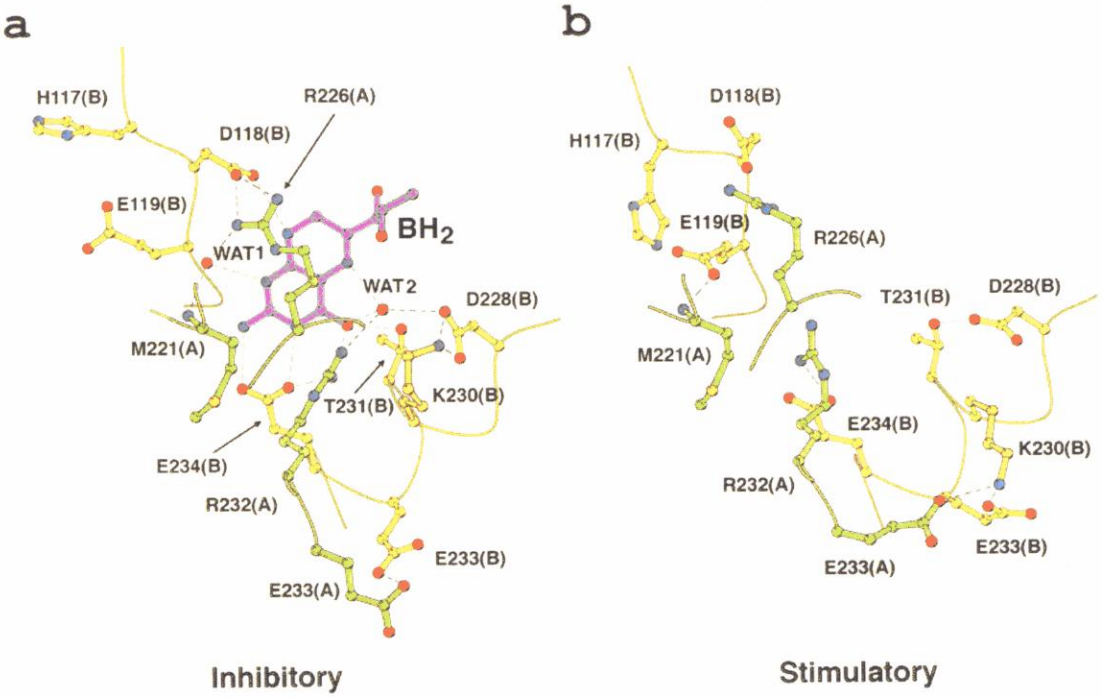

Figure 5-5. The BH_2-binding sites in the stimulatory (right) and the inhibitory (left) complexes. The parentheses after the residue name indicate the chain ID. The hydrogen bonding are indicated as dashed lines.

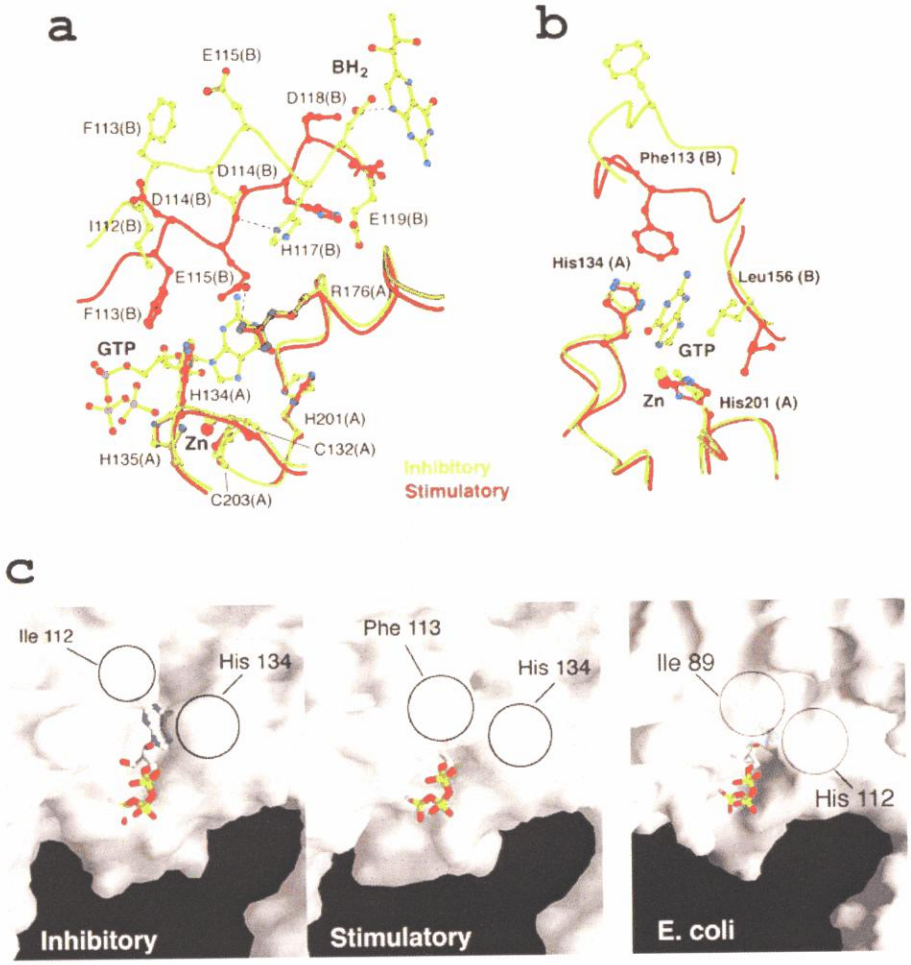

Figure 5-6. (a) Superimposition of the active sites in the stimulatory (red) and the inhibitory (green) complexes. The fitting calculations were done by using core β-barrel regions of GTPCHI pentemeric rings. The GTP molecule from the *E.coli* GTPCHI-GTP structure (PDB code 1A9C) is fitted on the structures. (b) The 90° rotated views from (a). (c) The molecular surfaces of the GTP binding site in the inhibitory (left), the stimulatory (middle) and the *E. coli* (right) GTPCHI, with the GTP molecule from the *E. coli* complex is overlayed.

Discussion

6-1. The inhibitory mechanism of GTPCHI-GFRP complex.

As observed in the *E. coli* and human GTPCHI structures, each rat GTPCHI monomer contains one zinc ion, which binds the conserved Cys^{132}, His^{135}, and Cys^{203} residues at the active site (Fig. 4-14). Superimposition of the pentamers of these enzymes also gave a small rms deviation value of 1.07 Å, suggesting no significant structural changes at the active site (Fig. 4-14). Since the *E. coli* enzyme shows no cooperativity and thus only one active form exists, the structural similarity observed between the *E. coli* GTPCHI and rat GTPCHI in the stimulatory complex suggests that GFRP locks the enzyme in the active form. In contrast, local structural changes at the GTP-binding site are found to be induced by BH_2-binding. In these structural changes, Phe^{113} and Leu^{156} play key roles to regulate the catalysis.

Recent biochemical studies have suggested the details of each reaction step as well as roles of key residues, as summarized in figure 6-1. It has been shown with *E. coli* H179A GTPCHI that His^{179} (His^{201} in rat) is indispensable for the formic acid releasing step (intermediate **1** to intermediate **2**), and the conversion of GTP to

intermediate **1** is reversible [Bracher *et al.*, 1999]. The stopped-flow kinetics analysis have shown that the equilibrium constant between GTP and intermediate **1** may be inclined to the GTP side [Schramek *et al.*, 2001; Bracher *et al.*, 2001]. Therefore, to release the formic acid, it is necessary for the N7 atom of GTP to be close to the N^{ε} atom of His^{201} for receiving the hydrogen atom (Fig. 6-1). Since the positions of essential residues are not changed between rsGTPCHI and riGTPCHI, the reaction could progress to form intermediate **2** or dihydroneopterin triphosphate (NH_2P3), because the Amadori rearrangement reactions are likely to progress non-enzymatically [Higgins & Bunn 1981], as well as following ring closure and dehydration [Andrews *et al.*, 1969]. However, no decrease of the GTP concentration was observed in the inhibitory complex [Harada *et al.*, 1993; Yoneyama & Hatakeyama, 1998]. Therefore, the reaction should be inhibited before the formic acid releasing step.

When the GTP molecule from the *E. coli* GTPCHI-GTP structure (PDB code: 1A8R) is superimposed on the GTPCHI-GFRP complexes, the distance between the N7 atom of GTP and the N^{ε} atom of His^{201} was found to be approximately 3.7 Å in both structures. This value is still longer to give the hydrogen from to the N^{ε} atom of His^{201} to the N7 atom of GTP. Therefore, the shift of Leu^{156} of GTPCHI in the inhibitory complex

may be important for the inhibition because Leu^{156} would block the guanine ring to approach toward the His^{201} N^{ε} atom. In the stimulatory complex, Leu^{156} is away for the guanine ring. Moreover, Phe^{113} play as a lid of the GTP-binding pocket (Fig. 6-2).

The regulatory mechanisms of the GTPCHI-GFRP complexes, supposed by comparing two-state structures are as follows; in stimulatory complex, the lid of the GTP-binding cavity (His^{134} and Phe^{113}) is closed, and the prop (Leu^{156}) is pulled back, so that the GTP N7 atom can interact with His^{201} N^{ε} atom. In inhibitory complex, although no change is observed in chain A, the large structural changes are occurred in chain B. The lid of cavity (Phe^{113}) is open, and the prop (Leu^{156}) is popped inside the cavity, interrupting the GTP N7 atom to access His^{201} N^{ε} atom (Fig. 6-2).

6-2. Allosteric Regulation of GTPCHI-GFRP

Allosteric regulations are seen at various proteins such as carrier proteins, ion channels, glycolyses and oxygen transfer. The allosteric proteins are usually oligomeric and have multiple ligand binding sites. The allosteric proteins usually have two forms, a low-affinity, poorly active form (the Tense-state) and a high-affinity, highly active form (the Relaxed-state). Most of the cases, the

conversion T-state to R-state (R-state to T-state as well) is occurred by ligand binding, and the ligand and/or substrate binding sites are located at subunit-subunit interfaces. The T-R transition is usually found as quaternary level, so it is able to affect in ligand binding sites, even if they are remote [Perutz, 1989; for reviews].

In this structural study of two states of the GTPCHI-GFRP complex, a large structural change at residue 106-115 of GTPCHI was observed (Fig. 5-6a), and this change directly affects to the GTP-binding (Fig. 5-6b). The allosteric regulation mechanism of the GTPCHI-GFRP complex is quite similar to those regular allosteric proteins, but several features are unique in this enzyme.

One of the unique features is that the substrate GTP is necessary for the inhibitory complex formation [Harada *et al.*, 1993; Yoneyama & Hatakeyama, 1998]. Most recent work has indicated that GTP is not always necessarily for the formation of the inhibitory complex, but enhancing the BH_4-binding [Yoneyama & Hatakeyama, 2001]. At pH 6.0, BH_4 alone fully induces the formation of the inhibitory complex. Crystallization of the inhibitory complex was carried out at pH 6. This might be the reason why deoxy-GTP molecules were not clearly detected in the crystal structure. The pH dependency of GTPCHI activity shows that the optimum pH for the catalysis is near 9.0 [Hatakeyama

et al., 1989].

Another feature is that the L-phenylalanine decreases the Hill coefficient of GTP from 1.85 to 1.0, resulting in enhancing the enzyme activity at low a GTP concentration [Harada *et al.*, 1993]. In the GFRP-free state, GTPCHI forms a functional decamer exhibiting the enzyme activity. Since the GTP-binding site is located at the interface of three subunits, the binding stoichiometry should be affected significantly by subunit-subunit interactions and mobility. Because the GFRP pentamer has a rigid structure, the binding of GFRP to GTPCHI may contribute to decrease the mobility of GTPCHI subunits.

The allosteric conversion mode of GTPCHI-GFRP complex is fitted on MWC (Monod-Wyman-Changeux) [Monod *et al.*, 1965] model rather than KNF (Koshland-Nemethy-Filmer) [Koshland *et al.*, 1966] model. The concentration of BH_4 and phenylalanine in rat liver are estimated to be 6 μM, 150 μM respectively. These values are comparable to the EC_{50} values of these ligands [Harada *et al.*, 1993].

In physiological conditions, BH_4 and phenylalanine are present at the same time. Conversion of T-state <-> R-state in physiological conditions, and how to exchange (or coexist) the ligands in complex will be the next issues.

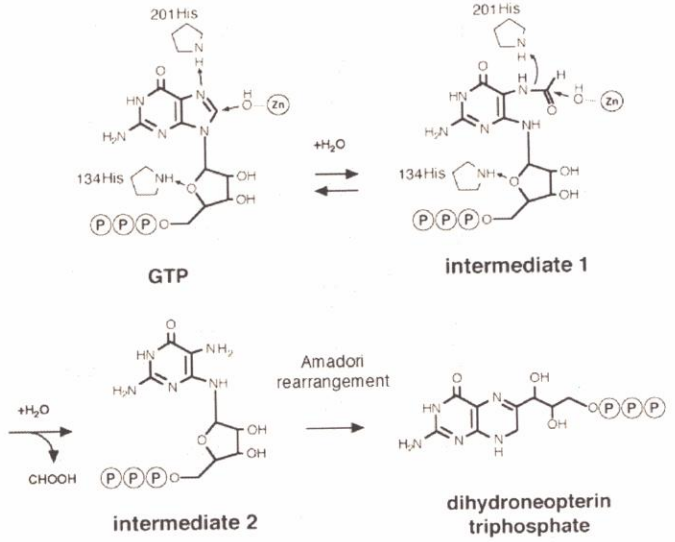

Figure 6-1. The reaction scheme of GTPCHI catalysis proposed from the mutation and the crystallographic studies of eGTPCHI. The residues of His^{201} and His^{134} act as protein donors in guanine ring-opening and formic acid releasing step.

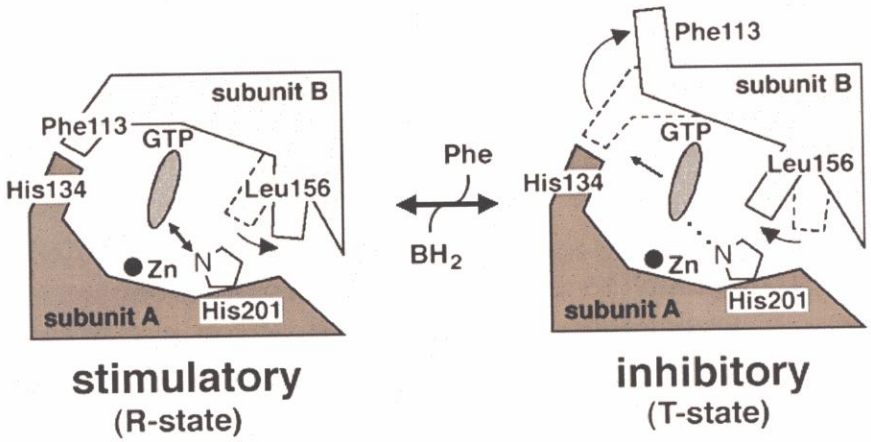

Figure 6-2. A model proposed from the crystal structure of the human and *E. coli* GTPCHI [Auerbach *et al.*, 2000], and the stimulatory and inhibitory GTPCHI-GFRP complex. In stimulatory complex, the lid of the GTP-binding pocket is closed, and Leu^{156} is pulled back. In inhibitory complex, the lid of cavity is widely open, and the Leu^{156} is popped inside the cavity, resulting that the GTP N7 atom is hard to access to His^{201} N^{ε} atom.

Supplemental Data

a. Abbreviations

GTPCHI, GTP cyclohydrolase I; GFRP, GTPCHI feedback regulatory protein; rsGTPCHI, rat stimulatory GTPCHI; riGTPCHI, rat inhibitory GTPCHI; eGTPCHI, *E. coli* GTPCHI; hGTPCHI, human GTPCHI; Phe, L-phenylalanine; BH_2, 7,8-dihydrobiopterin; BH_4, (6*R*)-L-erythro-5,6,7,8-tetrahydrobiopterin; MPD, 2-methyl-2,4-pentanediol; IPA, isopropyl alcohol.

b. Materials

Rat GTPCHI and GFRP were provided by Dr. K. Hatakeyama [Yoneyama *et al.*, 1997; Yoneyama & Hatakeyama, 1998]. Deoxy-GTP was purchased from Sigma, BH_2 was gifted from Dr. K. Hatakeyama. MPD and IPA were purchased from Wako pure chemical (Osaka, Japan). All equipments used for protein crystallography were purchased from Hampton research (California, USA).

c. Quantitative Analysis

Protein concentration were measured by the absorbance spectra with Beckman DU 640 spectrophotometer, with the extinction coefficients of the GTPCHI, GFRP and complex as E_{m280} = 1.64, 0.90 and 1.23 mL mg^{-1} cm^{-1}, respectively. Concentration of deoxy-GTP and BH_2 were measured in 0.1 N HCl solution by the absorbance spectra with the molar extinction coefficients as ε_{M252} = 12,200 and ε_{M255} = 11,000 M^{-1} cm^{-1}, respectively.

d. Figure Drawing

The figures were drawn with the following programs; *MOLSCRIPT* [Kraulis, 1991], *Raster3D* [Merritt & Bacon, 1997], *GRASP* [Nicholls *et al.*, 1991], *O* [Jones et al., 1991] and *RasMol* [www.bernstein-plus-sons.com/software/rasmol].

e. Publications

Maita, N., Okada, K., Hirotsu, S., Hatakeyama, K. & Hakoshima, T. (2001). Preparation and crystallization of the stimulatory and inhibitory complex of GTP cyclohydrolase I and its feedback regulatory protein GFRP. *Acta Crystallographica section D*, **57**, 1153-1156.

Maita, N., Okada, K., Hatakeyama, K. & Hakoshima, T. (2002). Crystal structure of the stimulatory complex of GTP cyclohydrolase I and its feedback regulatory protein GFRP. *Proceedings of the National Academy of Sciences USA*, **99**, 1212-1217.

f. Database Depositions

CRYSTAL STRUCTURE OF RAT GTPCHI/GFRP STIMULATORY COMPLEX
Protein Data Bank Code 1IS7

CRYSTAL STRUCTURE OF RAT GTPCHI/GFRP STIMULATORY COMPLEX PLUS ZN
Protein Data Bank Code 1IS8

Acknowledgements

This work has been performed under the direction of Professor Toshio Hakoshima (Division of Structural Biology, Nara Institute of Science and Technology). The author would like to express his deep gratitude to all members who belong(ed) to the Hakoshima laboratory; especially to Drs. T. Shimizu, K. Okada, K. Ihara and Hamada for technical support for structural analyses, to Drs. S. Hirotsu for protein crystallization. The author also wishes to thank Drs. K. Hatakeyama and T. Yoneyama (University of Pittsburgh) for providing the precious protein samples and biological comments during the study. The author also expresses his appreciation to Prof. N. Sakabe (Univ. of Tsukuba, TARA project), Dr. M. Suzuki and Dr. N. Igarashi (KEK) for supporting the data collection at Photon Factory, Dr. M. Kawamoto (JASRI) for supporting the data collection at SPring-8.

Finally, the author would like to say thank you to his parents who supported at every phase to their unworthy son.

References

Adams, J., Kelso, R. & Cooley, L. (2000). The kelch repeat superfamily of proteins: propellers of cell function. *Trends in Cell Biology*, **10**, 17-24.

Andrews, K.J.M., Barber, W.E. & Tong, P.B. (1969). *J. Chem. Soc.* **3**, 928-930.

Auerbach, G., Herrmann, A., Bracher, A., Bader, G., Gütlich, M., Fischer, M., Neukamm, M., Garrido, M.-F., Richardson, J., Nar, H. & Huber, R. (2000). Zinc plays a key role in human and bacterial GTP cyclohydrolase I. *Proceedings of the National Academy of Sciences USA*, **97**, 13567-13572.

Bader, G., Schiffmann, S., Herrmann, A., Fischer, M., Gütlich, M., Auerbach, G., Ploom, T., Bacher, A., Huber, R. & Lemm, T. (2001). Crystal structure of rat GTP cyclohydrolase I feedback regulatory protein, GFRP. *Journal of Molecular Biology*, **312**, 1051-1057.

Beisel, H.G., Kawabata, S., Iwanaga, S., Huber, R. & Bode, W. (1999). Tachylectin-2: crystal structure of a specific GlcNAc/GalNAc-binding lectin involved in the innate immunity host defense of the Japanese horseshore crab *Tachypleus tridentatus*. *EMBO Journal*, **18**, 2313-2322.

Bellahsene, Z., Dhondt, J.-L. & Rarriaux, J.-P. (1984). Guanosine triphosphate cyclohydrolase activity in rat tissues. *Biochemical Journal*, **217**, 59-65.

Bracher, A., Eisenreich, W., Schramek, N., Ritz, H., Götze, E., Herrmann, A., Gütlich, M. and Bacher, A. (1998). Biosynthesis of pteridines. NMR studies on the reaction mechanisms of GTP cyclohydrolase I, pyruvoyltetrahydropterin synthase, and sepiapterin reductase. *Journal of Biological Chemistry*, **273**, 28132-28141.

Bracher, A., Fischer, M., Eisenreich, W., Ritz, H., Schramek, N., Boyle, P., Gentili, P., Huber, R., Nar, H., Auerbach, G. & Bacher, A. (1999). Histidine 179 mutants of GTP cyclohydrolase I catalyze the formation of 2-amino-5-formylamino-6-ribofuranosylamino-4(*3H*)-pyrimidinone triphosphate. *Journal of Biological Chemistry*, **274**, 16727-16735.

Bracher, A., Schramek, N. & Bacher, A. (2001). Biosynthesis of pteridines. Stopped-flow kinetic analysis of GTP cyclohydrolase I. *Biochemistry*, **40**, 7896-7902.

Brique, S., Destée, A., Lambert, J.-C., Mouroux, V., Delacourte, A., Amouyel, P. & Chartier-Harlin, M.-C. (1999). A new GTP-cyclohydrolase I mutation in an universal dopa-responsive dystonia familial form. *NeuroReport*, **10**, 487-491.

Brown, G.M. & Williamson, J.M. (1987). Biosynthesis of folic acid, riboflavin, thiamine, and pantothenic acid. In *Escherichia coli* and *Salmonella typhimurium. Cellular and Molecular Biology* (ed. Neidhardt, F.C., American Society for Microbiology, Washington DC, USA), vol. 1, pp 521-538.

Brünger, A.T., Adams, P.D., Clore, G.M., DeLano, W.L., Gros, P., Grosse, R.W.-K., Jiang, J. S., Kuszewski, J., Nilges, M., Pannu, N. S., Read, R. J., Rice, L. M., Simonson, T. & Warren, G. L. (1998). *Crystallography & NMR System*: A New Software Suite for Macromolecular Structure Determination. *Acta Crystallographica Section D*, **54**, 905-921.

Burg, A.W. & Brown, G.M. (1966). The biosynthesis of folic acid. VI. Enzymatic conversion of carbon atom 8 of guanosine triphosphate to formic acid. *Biochimica et Biophysica Acta*, **117**, 275-278.

Burg, A.W. & Brown, G.M. (1968). The biosynthesis of folic acid VIII. Purification and properties of the enzyme that catalyzes the production of formate from carbon atom 8 of guanosine triphosphate. *Journal of Biological Chemistry*, **243**, 2349-2358.

Collaborative Computational Project, Number 4. (1994). The *CCP*4 suite: programs for protein crystallography. *Acta Crystallographica Section D*, **50**, 760-763.

Colloc'h, N., Poupon, A. & Mornon, J.-P. (2000). Sequence and structural features of the T-fold, an original tunneling building unit. *Proteins: Structure Function and Genetics*, **39**, 142-154.

Cort, J.R., Koonin, E.V., Bash, P.A. & Kennedy, M.A. (1999). A phylogenetic approach to target selection for structural genomics: solution structure of YciH. *Nucleic Acids Reserch*, **27**, 4018-4027.

Fülöp, V. & Jones, D.T. (1999). β propellers: structural rigidity and functional diversity. *Current Opinion in Structual Biology*, **6**, 715-721.

ter Haar, E., Musacchio, A., Harrison, S.C. & Kirchhausen, T. (1998). Atomic structure of clathrin: a beta propeller terminal domain joins an alpha zigzag linker. *Cell*, **95**, 563-573.

Harada, T., Kagamiyama, H. & Hatakeyama, K. (1993). Feedback regulation mechanisms for the control of GTP cyclohydrolase I activity. *Science*, **260**, 1507-1510.

Hatakeyama, K., Harada, T., Suzuki, S., Watanabe, Y. & Kagamiyama, H. (1989). Purification and characterization of rat liver GTP cyclohydrolase I. Cooperative binding of GTP to the enzyme. *Journal of Biological Chemistry*, **264**, 21660-21664.

Hendrickson, W.A. (1991). Determination of macromolecular structures from anomalous diffraction of synchrotron radiation. *Science*, **254**, 51-58.

Higgins, P.J. & Bunn, H.F. (1981). Kinetic analysis of the nonenzymatic glycosylation of hemoglobin. *Journal of Biological Chemistry*, **256**, 5204-5208.

Holm, L. & Sander, C. (1993). Protein structure comparison by alignment of distance matrices. *Journal of Molecular Biology*, **233**, 123-138.

Hope, H. (1988). Cryocrystallography of biological macromolecules: a generally applicable method. *Acta Crystallographica Section B*, **44**, 22-26.

Huang, Q., Teng, M. & Niu, L. (1999). Protein crystallization with a combination of hard and soft precipitants. *Acta Crystallographica Section D*, **55**, 1444-1448.

Ichinose, H., Ohye, T., Takahashi, E., Seki, N., Hori, T., Segawa, M., Nomura, Y., Endo, K., Tanaka, H., Tsuji, S., Fujita, K. & Nagatsu, T. (1994). Hereditary progressive dystonia with marked diurnal fluctuation caused by mutations in the GTP cyclohydrolase I gene. *Nature Genetics*, **8**, 236-242.

Jackson, R.J. & Shiota, T. (1975). The nature of the multiple forms of D-erythrodihydroneopterin triphosphate synthetase. *Biochimica et Biophysica Acta*, **403**, 232-244.

Jancarik, J. & Kim, S.H. (1991). Sparse Matrix Sampling : A Screening Method for Crystallization of Proteins. *Journal of Applied Crystallography*, **24**, 409-411.

Jones, T.A., Zou, J.Y., Cowan, S.W. & Kjeldgaard, M. (1991). Improved methods for binding protein models in electron density maps and the location of errors in these models. *Acta Crystallographica Section A*, **47**, 110-119.

Kaufman, S. (1997). Tetrahydrobiopterin - Basic Biochemistry and Role in Human Disease. (The Johns Hopkins University Press, Baltimore, USA).

Koshland, D.L., Nemethy, G. & Filmer, D. (1966). Comparison of experimental binding data and theoretical models in proteins containing subunits. *Biochemistry*, **5**, 365-385.

Kraulis, P.J. (1991). *MOLSCRIPT*: a program to produce both detailed and schematic plots of protein structures. *Journal of Applied Crystallography*, **24**, 946-950.

Laskowski, R.A., MacArthur, M.W., Moss, D.S. & Thornton, J.M. (1993). *PROCHECK*: a program to check the stereochemical quality of protein structures. *Journal of Applied Crystallography*, **26**, 283-291.

Laemmli, U.K. (1970). Cleavage of structural proteins during the assembly of the head of bacteriophage T4. *Nature*, **227**, 680-685.

Leslie, A.G. (1999). Integration of macromolecular diffraction data. *Acta Crystallographica section D*, **55**, 1696-1702.

Maita, N., Okada, K., Hirotsu, S., Hatakeyama, K. & Hakoshima, T. (2001). Preparation and crystallization of the stimulatory and inhibitory complex of GTP cyclohydrolase I and its feedback regulatory protein GFRP. *Acta Crystallographica section D*, **57**, 1153-1156.

Marletta, M.A. (1993). Nitric oxide synthase structure and mechanism. *Journal of Biological Chemistry*, **268**, 12231-12234.

Matthews, B.W. (1968). Solvent content of protein crystals. *Journal of Molecular Biology*, **33**, 491-497.

McCall, K.A., Huang, C.C. & Fierke, C.A. (2000). Function and mechanism of zinc metalloenzymes. *Journal of Nutrition*, **130(5S)**, 1437S-1446S.

McPherson, A. (1990). Current approaches to macromolecular crystallization. *Europian Journal of Biochemistry*, **189**, 1-23.

Meining, W., Bacher, A., Bachmann, L., Schmid, C., Weinkauf, S., Huber, R. & Nar, H. (1995). Elucidation of crystal packing by x-ray diffraction and freeze-etching electron microscopy. studies on GTP cyclohydrolase I of *Escherichea Coli*. *Journal of Molecular Biology*, **253**, 208-218.

Merritt, E.A. & Bacon, D.J. (1997). Raster3D: photorealistic molecular graphics. *Methods in Enzymology*, **277**, 505-524.

Milstein, S., Jaffe, H., Kowlessur, D. & Bonner, T.I. (1996). Purification and cloning of the GTP cyclohydrolase I feedback regulatory protein, GFRP. *Journal of Biological Chemistry*, **271**, 19743-19751.

Monod, J., Wyman, J. & Changeux, J.P. (1965). On the nature of allosteric transitions: A plausible model. *Journal of Molecular Biology*, **12**, 88-118.

Murzin, A.G., Brenner, S.E., Hubbard, T. & Chothia, C. (1995). SCOP: a structural classification of proteins database for the investigation of sequences and structures. *Journal of Molecular Biology*, **247**, 536-540.

Nagatsu, T. & Ichinose, H. (1998). Molecular biology of hereditary dystonia. *No To Hattatsu*, **30**, 93-100.

Nar, H., Huber, R., Meining, W., Schmid, C., Weinkauf, S. & Bacher, A. (1995a). Atomic structure of GTP cyclohydrolase I. *Structure*, **3**, 459-466.

Nar, H., Huber, R., Auerbach, G., Fischer, M., Hösl, C., Ritz, H., Bracher. A., Meining, W., Eberhardt, S. and Bacher, A. (1995b). Active site topology and reaction mechanism of GTP cyclohydrolase I. *Proceedings of the National Academy of Sciences USA*, **92**, 12120-12125.

Navaza, J. (1994). AMoRe: an automated package for molecular replacement. *Acta Crystallographica Section A*, **50**, 157-163.

Nicholls, A., Sharp, K. & Honig, B. (1991). Protein folding and association: insights from the interfacial and thermodynamic properties of hydrocarbons. *Proteins: Structure Function and Genetics*, **11**, 281-296.

Otwinowski, Z. & Minor, W. (1997). Proceeding of X-ray diffraction data collected in an oscillation mode. *Methods in Enzymology*, **276**, 307-326.

Perutz, M.F. (1989). Mechanism of cooperatively and allosteric regulation in proteins. (Cambridge University Press, Cambridge, UK).

Reynolds, J.J. & Brown, G.M. (1964). *Journal of Biological Chemistry*, **240**, 4449-4453.

Schramek, N., Bracher, A. and Bacher, A. (2001). Ring opening is not rate-limiting in the GTP cyclohydrolase I reaction. *Journal of Biological Chemistry*, **276**, 2622-2626

Shen, R., Alam, A. & Zhang, Y. (1988). Inhibition of GTP cyclohydrolase I by pterins. *Biochemica et Biophysica Acta*, **965**, 9-15.

Smith, T.F., Gaitatzes, C., Saxena, K. & Neer, E.J. (1999). The WD repeat: a common architecture for diverse functions. *Trends in Biochemical Science*, **24**, 181-185.

Sondek, J., Bohm, A., Lambright, D.G., Hamm, H.E. & Sigler, P.B. (1996). Crystal structure of a G_A protein $\beta\gamma$ dimer at 2.1 Å resolution. *Nature*, **379**, 369-374.

Sprague, E.R., Redd, M.J., Johnson, A.D., Wolberger, C. (2000). Structure of the C-terminal domain of Tup1, a corepressor of transcription in yeast. *EMBO Journal*, **19**, 3016-3027.

Thompson, J.D., Higgins, D.G. & Gibson, T.J. (1994). CLUSTAL W: improving the sensitivity of progressive multiple sequence alignment through sequence weighting, position-specific gap penalties and weight matrix choice. *Nucleic Acids Research*, **22**, 4673-4680.

Thöny, B., Auerbach, G. & Blau, N. (2000). Tetrahydrobiopterin biosynthesys, regeneration and functions. *Biochemical Journal*, **347**, 1-16.

Wolf, W.A., & Brown, G.M. (1969). The biosynthesis of folic acid X. Evidence for an Amadori rearrangement in the enzymatic formation of dihydroneopterin triphosphate from GTP. *Biochemica et Biophysica Acta*, **192**, 468-478.

Yoneyama, T., Brewer, J. M. & Hatakeyama, K. (1997). GTP cyclohydrolase I feedback regulatory protein is a pentamer of identical subunits. Purification, cDNA cloning, and bacterial expression. *Journal of Biological Chemistry*, **272**, 9690-9696.

Yoneyama, T. & Hatakeyama, K. (1998). Decameric GTP cyclohydrolase I forms complexes with two pentameric GTP cyclohydrolase I feedback regulatory proteins in the presence of phenylalanine or of a combination of tetrahydrobiopterin and GTP. *Journal of Biological Chemistry*, **273**, 20102-20108.

Yoneyama, T. & Hatakeyama, K. (2001). Ligand binding to the inhibitory and stimulatory GTP cyclohydrolase I/GTP cyclohydrolase I feedback regulatory protein complexes. *Protein Science*, **10**, 871-878.

Yim, J.J. & Brown, J.M. (1976). Characteristics of guanosine triphosphate cyclohydrolase I purified from *Escherichia coli*. *Journal of Biological Chemistry*, **251**, 5087-5094.